SPATIOTEMPORAL CONTROL OF HUMAN CARDIAC TISSUE THROUGH OPTOGENETICS

Stephen Ma

Submitted in partial fulfilment of the
requirements for the degree of
Doctor of Philosophy in the
Graduate School of Arts and Sciences

COLUMBIA UNIVERSITY

2018

ABSTRACT

Spatiotemporal Control of Human Cardiac Tissue Through Optogenetics

Stephen Ma

Cardiac arrhythmias are caused by disordered propagation of electrical activity. Progress in understanding and controlling arrhythmias requires novel methods to characterize and control the spatiotemporal propagation of electrical activity. We used patterned illumination of cardiomyocytes derived from optogenetic human induced pluripotent stem cells to create dynamic conduction blocks, and to test spatially extended control schemes. Using this model, we demonstrated the ability to initiate, circumscribe, relocate, and terminate pathologic spiral waves that drive many arrhythmias. When cells were derived from patients with long QT syndrome, longer action potential durations made spiral waves more resistant to termination. This work lays the foundation for personalized models of cardiac injury and disease, and the development of tailored approaches to the management of arrhythmias.

CONTENTS

LIST OF FIGURES

ACKNOWLEDGEMENTS

First and foremost I would like to thank my advisor, Professor Gordana Vunjak-Novakovic, to whom I am indebted for her unwavering support and generosity during my time in her laboratory. The intellectual freedom that she granted throughout my PhD was empowering and critical to my development as a researcher and scientist.

I would also like to thank the members of my thesis committee, Professor Elisa Konofagou, Professor Steven Marx, Professor Qi Wang, and Professor Masayuki Yazawa.

My partner in crime in all things optogenetics during my PhD was Olaia Fernandez Vila, who was a constant source of both technical guidance and scientific inspiration, and without whom this project would never have been successful. Credit also goes to Jinho Kim, who was instrumental in developing the optical hardware.

I also want to acknowledge Kacey Ronaldson, who welcomed me to the laboratory, Tim Chen, who has been on this journey with me from the beginning, Sue Halligan, who answered all of my weekend texts, and everyone else in the laboratory who enriched my PhD experience.

1 INTRODUCTION

1.1 Arrhythmias

Heart disease remains the leading cause of death in the United States, accounting for ~25% of total deaths [1]. Sudden cardiac death currently accounts for 400,000 deaths every year in the United States,[2] many of which can be attributed to a variety of arrhythmias, which are disorders in the propagation of electrical activity in the heart. Due to the intrinsically spatiotemporal nature of arrhythmias, their behavior depends critically on the geometry and electrophysiological properties of the myocardial substrate. In particular, the normal orderly propagation of planar wavefronts through the heart can be perturbed through anatomic[3] and electrophysiological defects,[4,5] leading to aberrant waveforms such as spirals that can drive tachycardia and fibrillation.

1.2 Reentry

Arrhythmia mechanisms can be divided along a number of different axes. We focus here on the distinction between reentrant and nonreentrant activity. Nonreentrant arrhythmias include those caused by focal activity such as enhanced automaticity or triggered activity. Reentry occurs when propagating action potentials fail to extinguish and instead reactivates a region that has recently returned to a resting state. Reentry can be further divided into two types: anatomic and functional. The theoretical and experimental background for the modern understanding of reentry as a self-sustaining dynamic equilibrium dates back to 1887,[6] with additional publications following after the turn of the century.

1.2.1 Anatomic reentry

Anatomic reentry can be described as the unidirectional circulation of electrical activity around a ring of cardiac tissue. Inspired by similar experiments performed in jellyfish in 1906,[7] G. R. Mines demonstrated the first instance of what was later termed the 'circus movement hypothesis of reentry' in cardiac tissue in 1913. He showed that self-sustaining unidirectional waves of contraction could circulate indefinitely around rings cut from tortoise hearts (**Figure 1.1**), and suggested that they could form the basis for cardiac fibrillation.[8] Today, we know that anatomically defined reentry is related to a number of different arrhythmias with various mechanisms, such as the presence of accessory pathways in Wolf-Parkinson-White, or by the presence of scar tissue secondary to myocardial infarction.[9] Anatomic reentry requires that the cycle length for a wavefront traveling around the circuit must be longer than the refractory period, such that the wave does not collide with itself and extinguish.

Figure 1.1 Heart ring used by Mines to demonstrate anatomic reentry, and accompanying illustrations of reentrant circuits[8]

1.2.2 Functional reentry

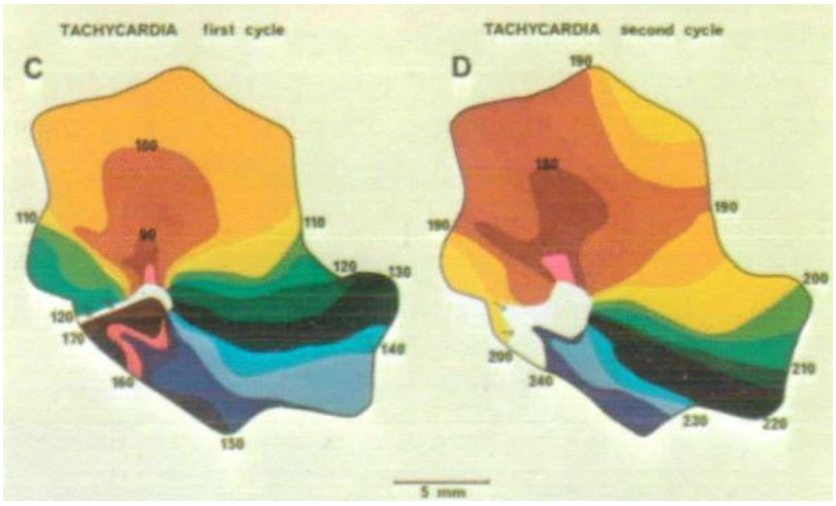

Figure 1.2 Functional reentry documented by Allessie et al[10]

In contrast to anatomic reentry, functional reentry occurs without the presence of an anatomic obstacle. Functional reentry was first demonstrated in 1973 by Allessie et al (**Figure 1.2**),[10] though conceptually it had been suggested several decades prior in parallel with the experimental work demonstrating anatomic reentry.[11] A follow-up paper in 1977 introduced the "leading circle hypothesis" to explain re-entrant activity without an anatomic obstacle (**Figure 1.3**).[12] This theory postulated that functional reentry occurred around a functional obstacle, which was maintained in a permanently refractory state due to encroaching waves from the circulating wave. In comparison to anatomic reentry, the period of rotation is defined not by the path length, but by the intrinsic electrophsyiologic properties of the tissue governing the conduction velocity and refractory period. While promising, this theory was ultimately supplanted as it was unable to adequately explain the dynamics of fibrillation, particularly the drift and meander of the circulating wave front that is precluded by the presence of a stationary, permanently refractory functional obstacle.

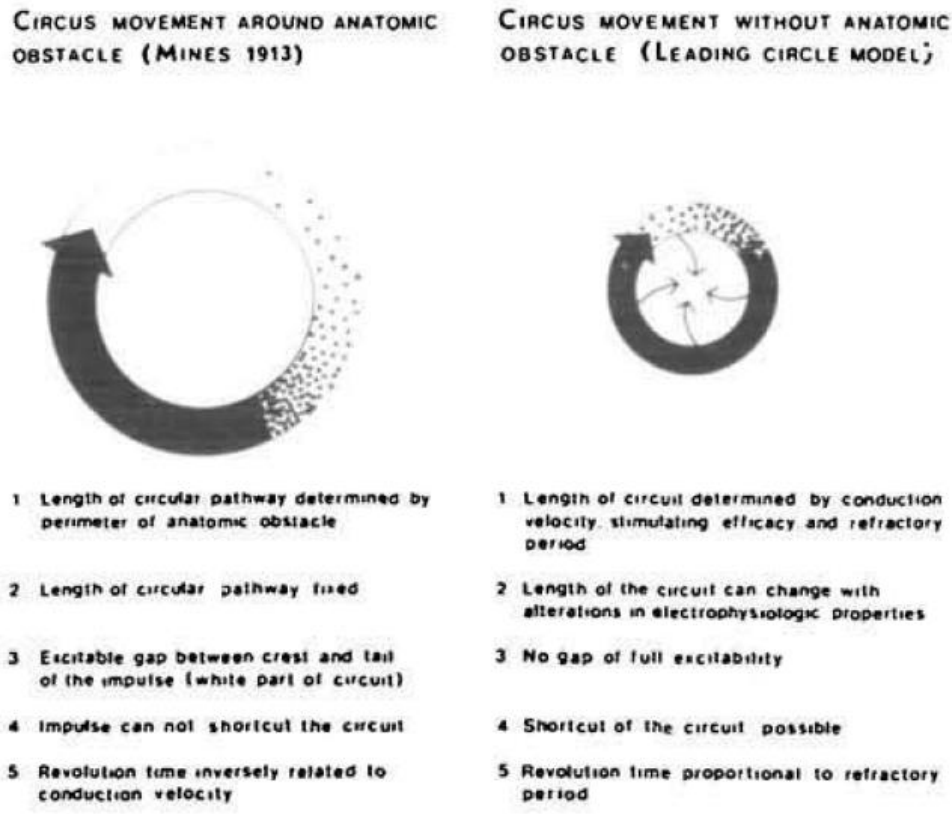

Figure 1.3 Leading circle hypothesis[12]

Further insight would eventually arrive from the study of similar vortex-like phenomena found in other types of excitable media, termed spiral waves in two-dimensional substrates.[13] A general mathematical theory for the behaviour of spiral waves in excitable media has been established using insights gained from this collection of systems. Spiral waves are governed by the relationship between the current source (excited cells at the leading edge of the wave) and the current sink (the quiescent, excitable cells just beyond the wavefront). The smaller the source-sink ratio, the lower the conduction velocity, and the shorter the action potential duration. This mismatch is greatest at the tip of the spiral, and gradually diminishes along the length of the wave. The gradient in conduction velocity goes hand-in-hand with the convex curvature of the wave, with the greatest curvature and lowest conduction velocity at the center of the spiral, where the value of the source-sink relationship is critical, and excitation fails. This leaves an excitable, but nonexcited core also known as the phase singularity (**Figure 1.4**), since all phases meet at this location.[14] It is generally understood that the phase singularity acts as the source of the spiral wave since elimination of the phase singularity is necessary and sufficient for elimination of the corresponding spiral wave. The source of the spiral is also termed a rotor, though in practice the terms rotor, phase singularity, and spiral wave are used interchangeably.

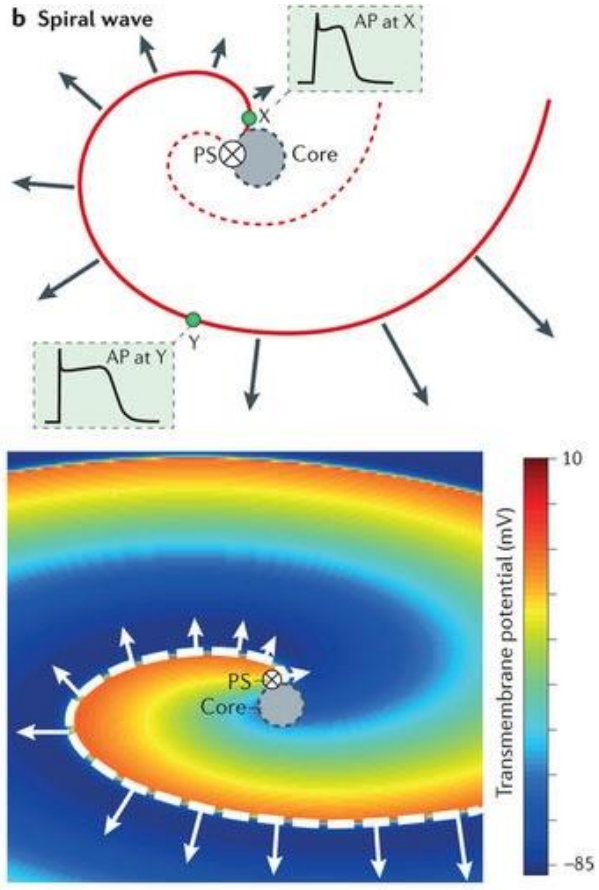

Figure 1.4: Spiral wave schematic[14]

1.3 Initiation and termination of reentry

The characterization of reentry above as a dynamic equilibrium implies a steady state once reentry is established. However, we must be able to enter and exit from this equilibrium. The mechanisms are heterogeneous and varied, but a short discussion of simple cases is warranted.

1.3.1 Initiation and termination of anatomic reentry

As previously discussed, anatomic reentry requires the presence of multiple paths with sufficient length. Additionally, initiation of anatomic reentry also requires the presence of unidirectional conduction block on one of the paths. This can occur through a confluence of geometric and electrophysiologic factors as illustrated below (***Figure 1.5***).[15,16]

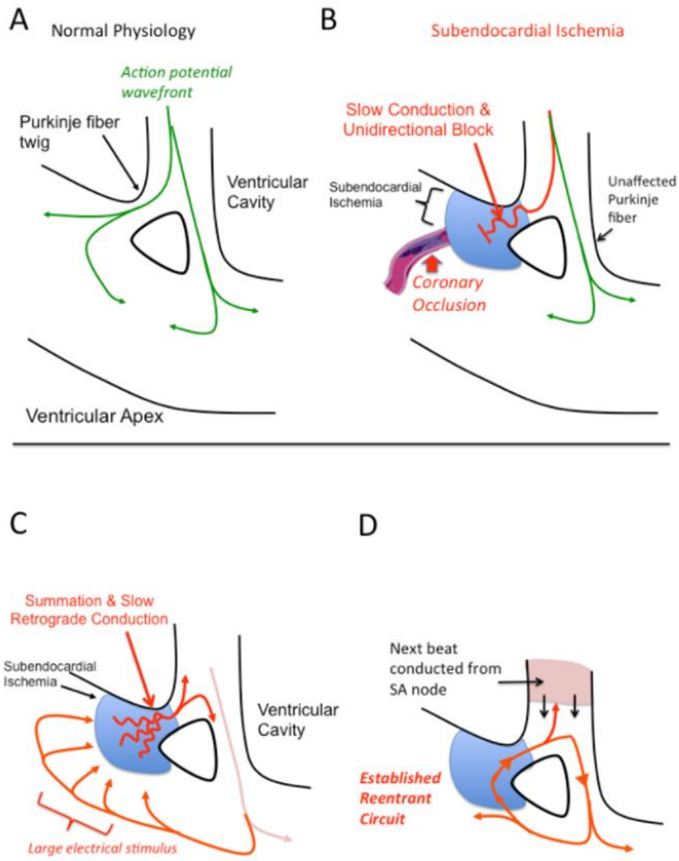

Figure 1.5 Unidirectional block and reentry initiation (adapted from the Cellular Basis for Cardiac Arrhythmias,[15] which modified a figure from BG Katzung's Basic and Clinical Pharmacology[16])

Termination of anatomic reentry requires destruction of the circulating waveform. This can be accomplished pharmacologically, such as by action potential duration elongation to increase the wavelength beyond the length of the circuit, or through external pacing directly interfere with the propagating wave. However, as long as the circuit exists, re-entrant activity is likely to recur. Permanent solutions often involve the use of catheter ablation to destroy the accessory pathway such as in the treatment of Wolff-Parkinson White.[17]

1.3.2 Initiation and termination of functional reentry

Spiral waves arise when the interaction of a wavefront with an obstacle leads to wavebreak, which generates the isolated tips necessary for spiral wave formation. In homogeneous media, this can be a transient functional obstacle created by the refractory wake of a previous wavefront, as seen in spiral wave induction through the S1-S2 stimulation protocol (also known as cross-field stimulation) (***Figure 1.6***).[18,19]

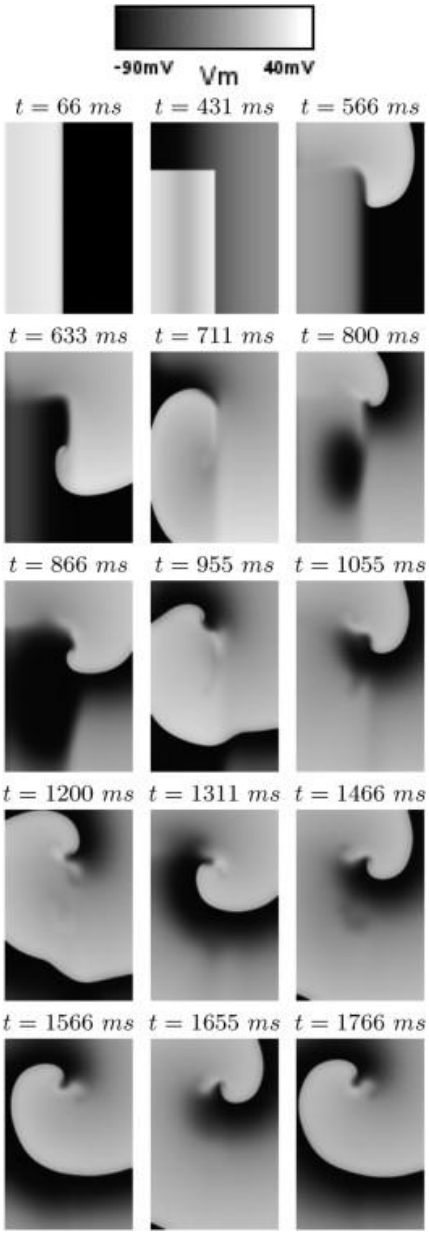

Figure 1.6 S1-S2 stimulus protocol induces wavebreak and spiral wave formation[18]

Anatomic heterogeneities, caused by the native structure of the heart or by pathologies such as myocardial infarctions or structural remodelling, can also induce wavebreak and spiral wave formation. A prominent experimental demonstration of wavefront instabilities caused by wave interactions with conduction blocks in heart tissue occurred in 1996, with the demonstration of vortex shedding in computational and *in vitro* monolayer experiments.[20] Insufficient wavefront curvature combined with source-sink mismatch created by specific anatomic heterogeneities leads to wave break, vortex shedding, and the formation of rotating

spiral waves (***Figure 1.7***),[21] also known as rotors, which are important contributors to both atrial and ventricular fibrillation.[22,23]

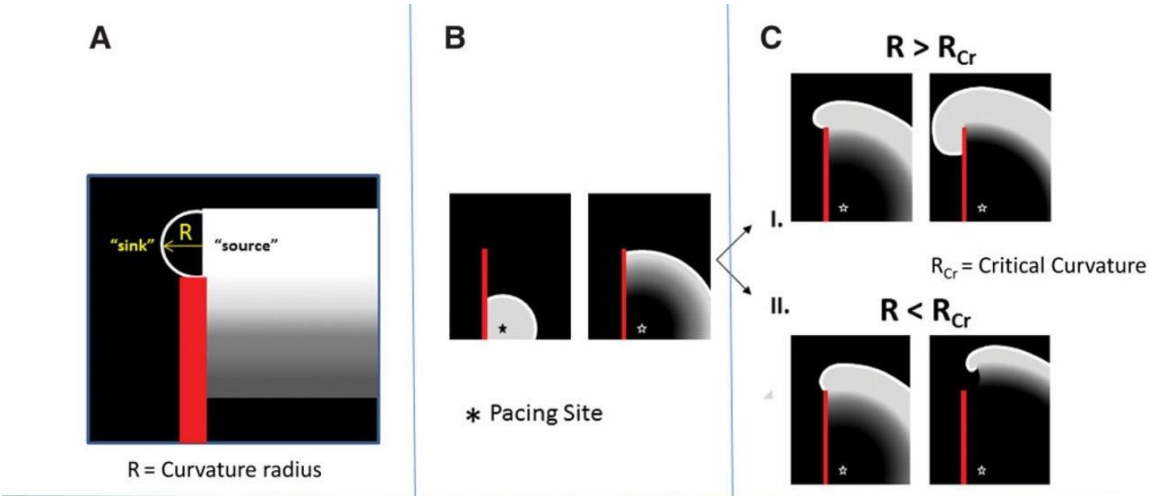

Figure 1.7 Vortex shedding when the radius of curvature R fails to exceed the critical curvature for detachment R_{Cr}.[21]

Similar to anatomic reentry, destruction of the wavefront through collision with another wavefront or a tissue boundary will result in reentry termination (***Figure 1.8***).[24] As the source of the spiral wave is the rotor, the termination of functional reentry can also be accomplished through elimination of the rotor, either through the influence of another wave (**Figure 1.9**),[24] through collision with an existing boundary (**Figure 1.9B**),[25] or through collision with another rotor (**Figure 1.9B**).[25]

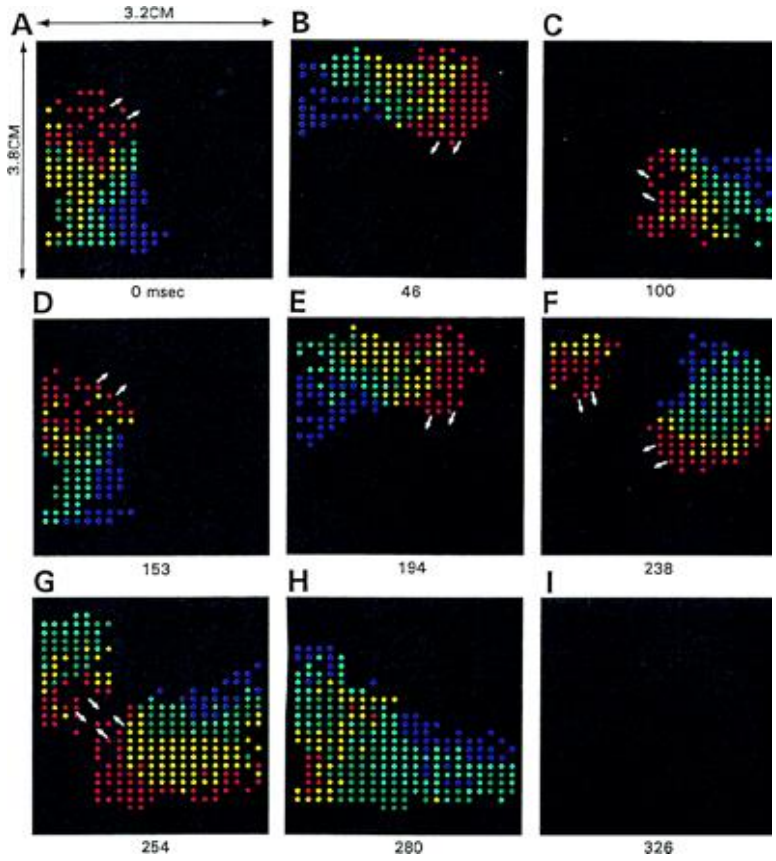

Figure 1.8 Reentry termination in isolated canine atrial tissue through wavefront collision[24]

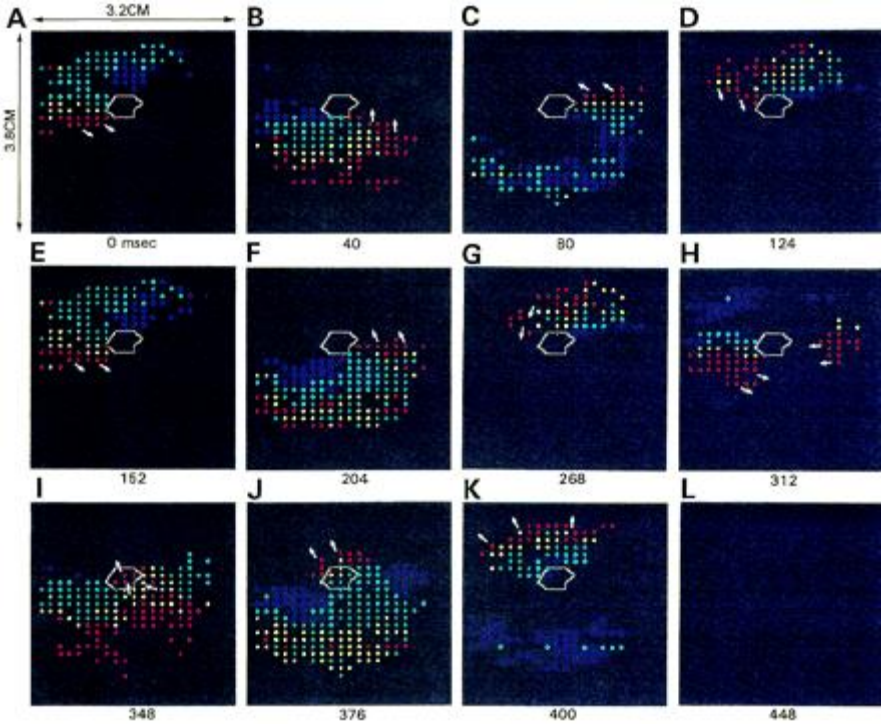

Figure 1.9 Reentry termination in isolated canine atrial tissue through core excitation[24]

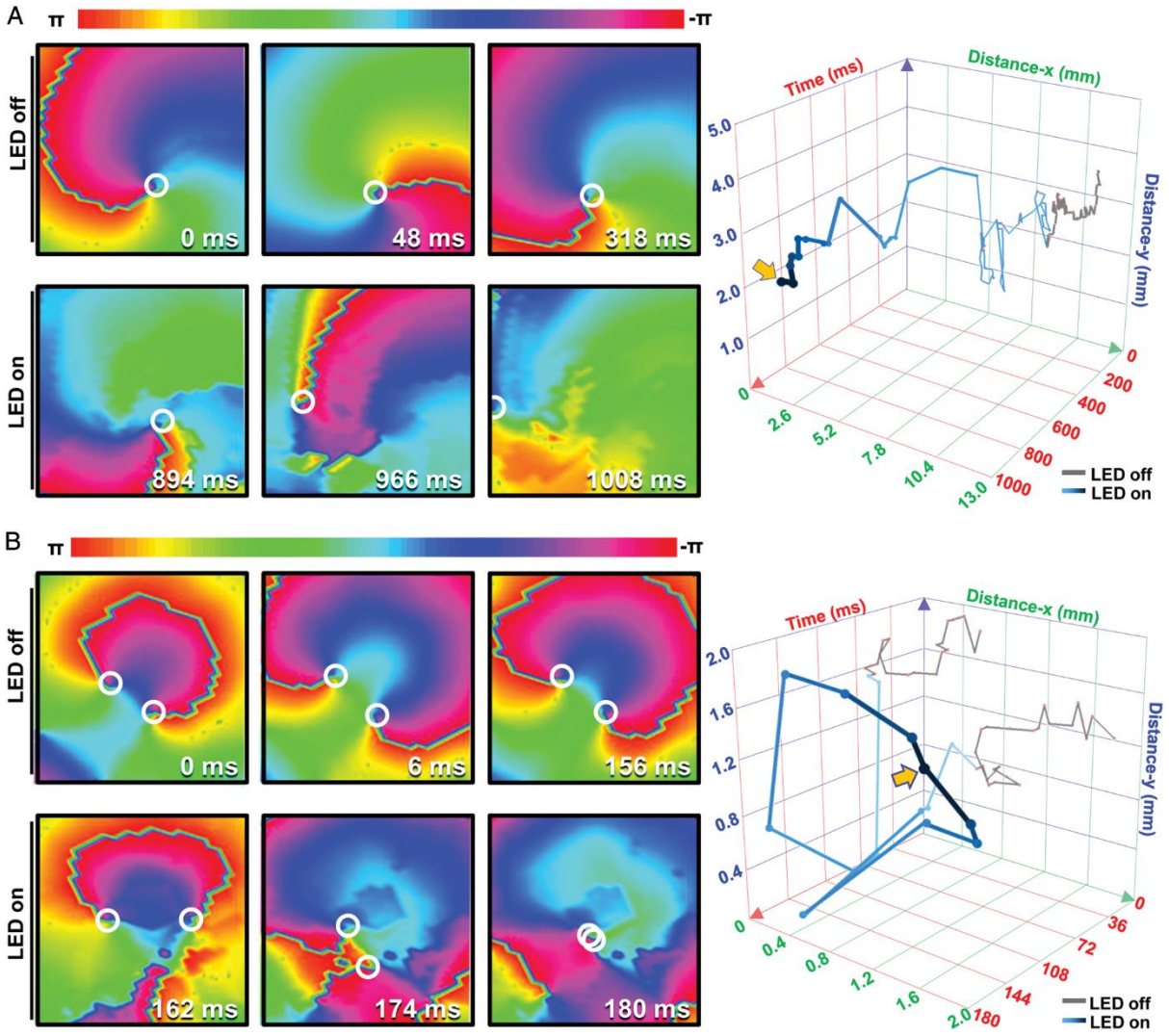

Figure 1.10 Reentry termination in neonatal rat atrial myocyte culture

(A) Phase singularity-boundary collision and (B) phase singularity-phase singularity collision secondary to light exposure of channelrhodopsin-expressing substrate.[25]

1.4 Limits to our understanding of reentry

Despite the undeniable progress over the past century in our understanding of reentrant activity, clinical progress in the management of patients with reentrant arrhythmias has been limited. Gaps continue to exist both in our understanding of the mechanisms underlying reentry, as well as in our ability to terminate and prevent reentrant activity. I focus here on two specific areas of interest, with significant clinical implications and which are

conceptually linked by an emphasis on the intrinsically spatiotemporal nature of reentrant activity: 1) what is the impact of substrate heterogeneity on the initiation, maintenance, and termination of reentry, and 2) how do we best manage reentrant activity?

1.4.1 The impact of substrate geometry on re-entrant activity

As discussed, the importance of conduction blocks and substrate heterogeneity has been recognized both conceptually and experimentally in our understanding of reentrant activity since the very first publications on the topic. We know that anatomic heterogeneity is responsible for phenomena such as spiral wave initiation, termination, and maintenance, as functional reentry can convert to anatomic reentry when rotors encounter anatomic heterogeneities of the appropriate size.[26,27] However, our understanding is fairly rudimentary, with an emphasis on simple examples such as circles or lines. We have not yet reached the stage where we are able to utilize our insights for clinical application.

One area of interest is the prediction of arrhythmia risk for specific scar patterns. One of the most recent publications in this area was the recently completed GAUDI-CRT study, which demonstrated the predictive value of scar heterogeneity, quantified as border zone mass on contrast-enhanced cardiac magnetic resonance imaging, for sudden cardiac death risk stratification in post-MI patients (**Figure 1.11**).[28] Its results complement previous studies, which showed similar results.[29–33] However, while promising, current studies say nothing about the specific shapes and structures that are pro-arrhythmogenic.

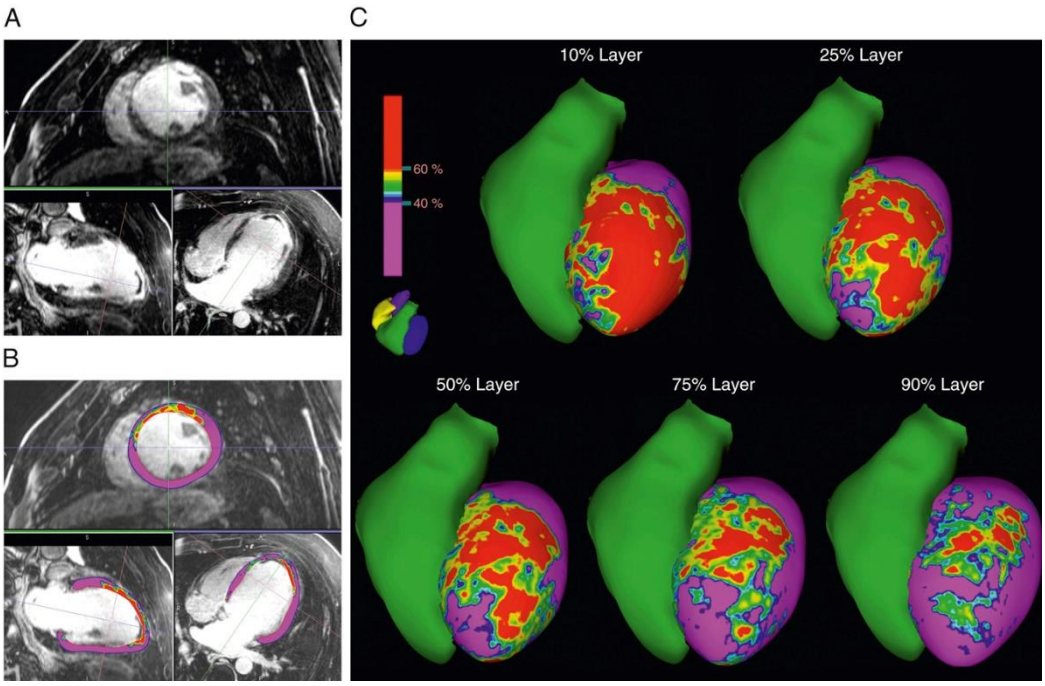

Figure 1.11 Contrast-enhanced cardiac magnetic resonance images segmented into scar (red), border zone (green), and healthy tissue (purple) based on signal intensity for the GAUDI-CRT study[28]

The ability to predict arrhythmogenicity as a function of scar shape and structure is particularly relevant in the context of catheter ablation. Catheter ablation is a technique whereby electrophysiologists use a catheter to create scar tissue in the heart as a treatment for specific arrhythmias. It is commonly used with success for ablation of accessory pathways in conditions such as Wolff-Parkinson White (WPW) Syndrome.[17] Catheter ablation can also be used for the treatment of ventricular tachycardias in the context of myocardial infarction, where it is used to ablate narrow isthmuses in the scar border zone. However, the success rate is much lower than that for WPW, and attempts to better stratify ablation candidates are ongoing.[34] We are again limited by our inability to correctly predict arrhythmia risk as a function of scar, particularly with respect to how modifications of scar geometry can ameliorate that risk. This is also true in the use of catheter ablation in the treatment of chronic atrial fibrillation, which is the most prevalent arrhythmia, and significantly increases the patient's risk of suffering a stroke. Here, catheter ablation is successfully used to isolate the pulmonary veins, which are the primary source of ectopic beats, but its success rate in atrial fibrillation that is refractory to pulmonary vein isolation is quite poor.[35,36]

Moreover, conduction blocks are only the most obvious manifestation of spatial heterogeneity in cardiac tissue. Ventricular dyssynchrony is an important risk factor for death and cardiac remodeling following a myocardial infarction, and is associated with mitral regurgitation,[37] while spatially heterogeneous action potential duration restitution and repolarization dispersion is linked with ventricular fibrillation, monomorphic ventricular tachycardia, and torsades de points.[38–43] Islands of midmyocardial cells are also linked to the development of torsades de pointes in long-QT syndrome.[44] Atrial fibrillation is associated with changes cardiac connectivity.[45] These isolated observations require further systematic study to develop a proper theory for cardiac behavior as a function of substrate geometry.

1.4.2 Methods to terminate reentry

Treatment of reentrant arrhythmias relies on two main treatment modalities. Pharmacological treatment globally modifies substrate electrophysiology, with mixed results depending on the type of arrhythmia.[46] For instance, pharmacological treatment for atrial tachyarrhythmias are often pro-arrhythmogenic in the ventricles, though there are now efforts to develop drugs that specifically target the atria.[47] In contrast to pharmacological treatment, external pacing is typically applied at a few select locations.[48,49] The MINERVA trial conducted in 2014 directly compared DDDRP vs DDDRP + MVP (DDDRP = atrial preventive pacing, atrial antitachycardia pacing, MVP = managed ventricular pacing). These algorithms are some of the most advanced algorithms in use, and yet they still only featured thze use of two leads: one in the atrium and one in the ventricle. Studies using multiple stimulation sites per chamber for various indications are still relatively infrequent, and there is little mechanistic insight in the choice of stimulation site.[50]

In spite of our best efforts, refractory arrhythmias persist in the face of optimal therapy. Conceptually, it appears that this can at least partially be attributed to the spatial simplicity of our available control schemes: either global pharmacological changes, or local pacing at a small handful of sites. The spatially heterogeneous pathologies mentioned in section 1.4.1 demand spatially targeted solutions. The only treatment that currently meets this definition is targeted catheter ablation for refractory arrhythmias,[35,36,51] which remains limited in scope and development as previously discussed. However, with the advent of technology such as flexible electrode arrays that could potentially provide hundreds of pacing locations,[52] optimization of spatially extended control schemes is a promising direction for research.

1.5 Computational insights

Attempts to better understand 1) the interaction between substrate heterogeneity and reentrant activity, and 2) how to best terminate reentry, are currently best approached using computational methods. For instance, a recent computational paper predicted a fractal-like pattern of the system's dynamic steady state (quiescent, single reentrant circuit, disorganized chaos) as a function of obstacle location in a cardiac monolayer, with minute changes in obstacle placement leading to dramatic differences in the behavior of the system (**Figure 1.12**).[53] While the exact pattern is an artifact of the parameters of the computational experiment (as can be deduced by the lack of symmetry), the existence of bifurcations in system behavior sensitive to initial conditions is expected in nonlinear systems like the heart.[20,54–56]

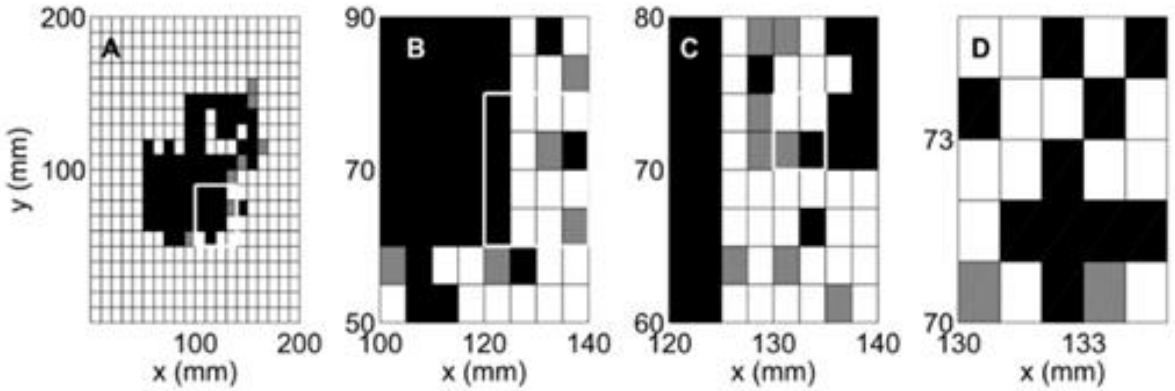

Figure 1.12 Fractal-like dependence of system response as a function of obstacle location.[53]

A 40mm x 40mm obstacle was placed in every location, and the resulting behavior was characterized. Squares represent behavior when the bottom-left corner of the obstacle was placed in that location: white is quiescence, black is a single rotating spiral, and gray is disorganized chaos. The boundary between the black and white regions exhibits a fractal-like pattern with qualitative changes in behavior for minute changes in initial conditions. This is characteristic for nonlinear, chaotic systems.

Computational studies have also identified a number of promising control schemes, such as grids and traveling waves **(Figure 1.13)**.[53,57–59] Similarly, they have also been used to hypothesize mechanisms for arrhythmia termination through the modification of substrate

geometry via catheter ablation.[60] Some studies have even looked at the robustness of theses spatiotemporal control schemes in the context of anatomic obstacles.[61] However, these results require validation in biological systems with similar spatiotemporal resolution and throughput.

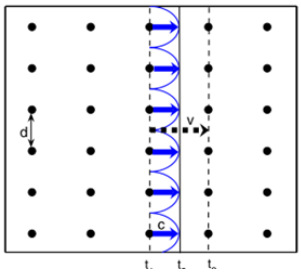

Figure 1.13 Computational simulation of a traveling wave created by an array of electrodes. Electrodes are distance d apart. The traveling wave moves with speed v. The speed of conduction in the simulated tissue is c.[62]

1.6 Limitations in current biological systems

Unfortunately, biological systems are much more difficult to manipulate than computational models. Traditional methods for anatomic manipulation of tissues include manual excision or injury,[20] 3D printing,[63] micropatterning,[64] and reliance on stochastic processes.[65,66] These methods are logistically involved, requiring hardware fabrication and the creation of new tissue samples for every iteration, and are technically limited in their precision. Consequently, large-scale experiments along the lines of the one shown in **Figure 1.12** have not been attempted in biological substrates.

Similarly, spatiotemporal control is only achievable by coupling the above with the laborious process of creating custom electrode arrays through photolithography, or the manual placement of electrodes. As a result, the only algorithms that have been studied in biological systems are local pacing algorithms at a handful of electrodes,[67] which constitutes a small corner of the experimental space.

1.7 Summary

In summary, while our understanding of reentry has greatly progressed over the past century, there are still significant gaps in our mechanistic understanding of how reentry is initiated,

maintained, and terminated, particularly in the context of anatomic heterogeneities. One of the factors holding back progress is our inability to easily translate hypotheses that are generated in computational models to biological systems. Further progress in this area would therefore be accelerated by the development of high-throughput biological systems that would allow us to 1) systematically characterize reentry as a function of substrate geometry, and 2) rapidly prototype novel control schemes.

2 Innovation, Approach, and Aims

2.1 Innovation

A number of recent advances in light-sensitive proteins and stem cell biology can now be combined with patterned illumination to enable precise spatiotemporal sensing and actuation of cellular membrane potential using optical systems.

2.1.1 Optogenetics

Optogenetics can be described as light-based actuation through genetic engineering. Light-sensitive ion channels such as channelrhodopsin (**Figure 2.1**)[68] or anion channelrhodopsin allow optical excitation/inhibition of excitable cells such as cardiomyocytes or neurons. The precise spatiotemporal control enabled by optogenetics makes it promising for in vitro applications in tissue engineering. In comparison with electrical stimulation, optogenetic stimulation has some interesting properties as it allows us to: (i) target specific cell types, (ii) both excite and inhibit targeted cells, and (iii) take advantage of miniaturized projectors to easily achieve high-resolution spatiotemporal control of excitable tissues in vitro.[69] The number of proteins available for optical sensing and actuation continues to increase as well, supporting both novel mechanisms of action as well as spectrally differentiated wavelengths for multiplexed sensing and stimulation.[70–74]

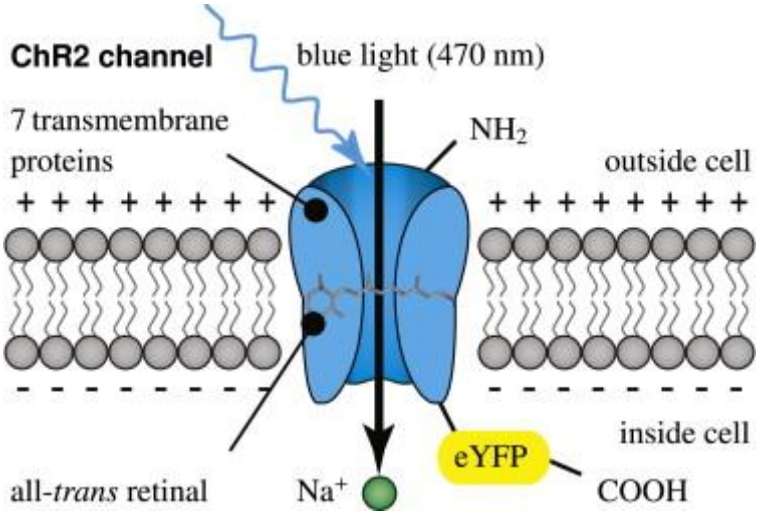

Figure 2.1 Channelrhodopsin[68]

2.1.2 Human induced pluripotent stem cells

On the biological side, the development of human induced pluripotent stem cell (hiPSC) technology allows for the generation of multiple cell types from the same cell line.[75–78] This property is most commonly used to facilitate the study of genetic diseases through the use of patient-derived cell lines,[79,80] but also lends itself to the development and use of transgenic stem cell lines through genetic engineering. These stem cell also lines serve as an unlimited source of human cells that are not readily available, such as human induced pluripotent stem cell-derived cardiomyocytes (hiPS-CMs).[81] For these reasons, hiPSCs and their differentiation products have been rapidly adopted for *in vitro* studies.

2.1.3 Patterned illumination and high-speed optical mapping

Finally, advanced optical systems are available for imaging and patterned illumination of biological systems with high spatiotemporal resolution.[69,82] In 2009, Fairchild Imaging, Andor Technology, and PCO together developed scientific CMOS (sCMOS) sensors characterized by high frame rates with high spatial resolution (100fps with full-frame resolution of 2048 x 2048 pixels), high quantum efficiency (>84%), and low noise. These cameras are ideal for optical mapping, which requires high speeds and spatial resolution while detecting the relatively weak fluorescent signals associated with voltage and calcium sensors.[83]

In the space of patterned illumination, there are a number of sptial light modulating technologies now available. For 2D projection, one of the most commonly used technologies are the digital micromirror devices (DMD) invented at Texas Instruments. Initially conceived as a deformable mirror device in 1977, the device evolved to its current, bistable switching form in 1987 (**Figure 2.2**).[84] It was finally commercialized in 1996 under the auspices of Digital Light Processing™ technology, and has since taken over a large portion of the projection display market.[84] This technology is uniquely suited for patterned illumination in the context of cardiac electrical activity, with modern DMDs offering millisecond temporal precision and greater than HD pixel counts.

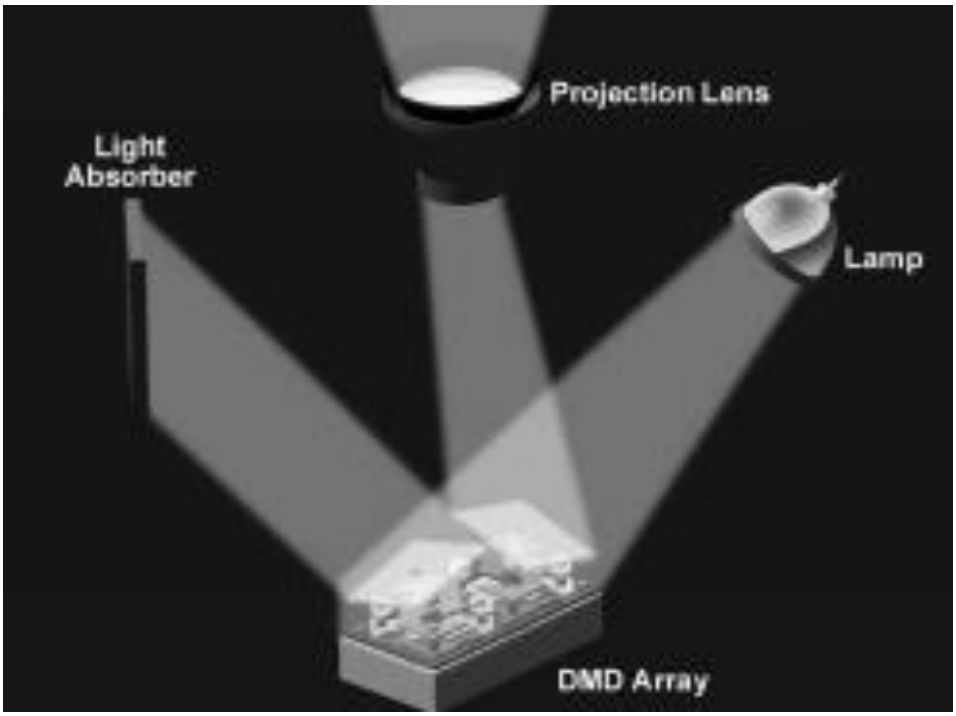

Figure 2.2 Digital Micromirror Device[84]

2.2 Hypothesis

We hypothesized that we could develop a novel *in vitro* platform using optogenetic methods for the characterization of reentrant activity as a function of substrate heterogeneity, and the validation of novel control schemes.

We created stable hiPSC lines expressing channelrhodopsin (ChR2), a cation channel that depolarizes the membrane in response to ~470nm light,[85] or anion channelrhodopsin 2 (*Gt*ACR2), an anion channel that hyperpolarizes the membrane in response to ~470nm

light.[71] These light-sensitive cardiac tissues will enable dose-dependent, spatially heterogeneous control of cell excitation through the use of patterned light. The light patterns will be created by integrating a projector into existing optical mapping systems, allowing for simultaneous imaging and stimulation. The end-result will be a system capable of controlling the spatiotemporal propagation of waves through cardiac tissue in real time (**Figure 2.3**). This approach would meet the experimental need described in **section 1.7**.

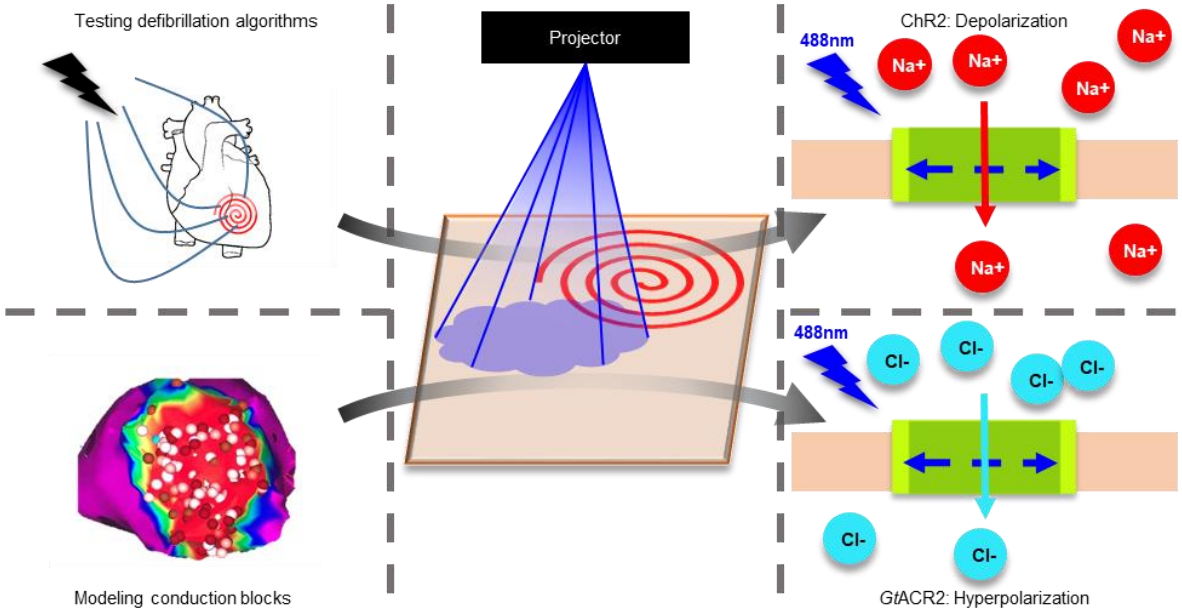

Figure 2.3 Graphical Abstract. Patterned illumination of optogenetic proteins allows for high-resolution spatiotemporal control of cardiac tissue.

Channelrhodopsin (ChR2) and anion channelrhodopsin 2 (GtACR2) are cation/anion channels that open in response to blue light, leading to membrane depolarization/hyperpolarization. The use of a projector in combination with these optogenetic proteins allows for easy, spatially extended, high-resolution control of transgenic cardiac tissue. We use ChR2 to test control algorithms, and use GtACR2 to model conduction blocks.

2.3 Relationship with control theory

Control algorithms for dynamically changing systems require closed-loop feedback, where sensors detect changes in the system, and that information is used to modify the actuation that the system receives in real-time. Closed-loop control where sensing information is routed

back into the control algorithm is superior to open-loop systems where feedback is not used. Abstractly, our approach can be conceptualized as the development of a control system with all-optical actuation and sensing for high-throughput *in vitro* modelling (**Figure 2.4)**.

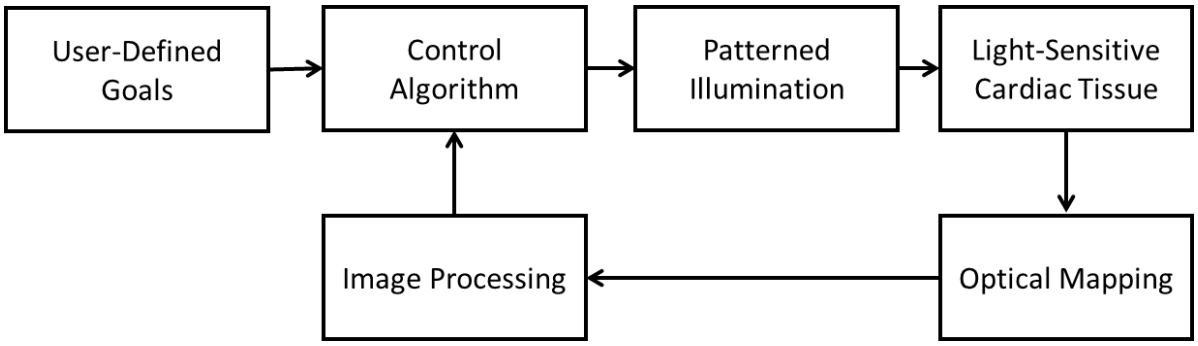

Figure 2.4 All-optical actuation and sensing control system

2.4 Experimental approach

We developed human stem cell lines expressing channelrhodopsin, a nonspecific cation channel that depolarizes the membrane in response to ~470nm light,[85] and anion channelrhodopsin, an anion channel that hyperpolarizes the membrane in response to ~470nm light.[86] Cardiomyocyte monolayers differentiated from these transgenic cell lines formed the substrate for patterned illumination and imaging. A projector was integrated into existing optical mapping systems, allowing for simultaneous imaging and stimulation. We then use this platform to systematically evaluate the efficacy of novel spatiotemporal control algorithms for arrhythmia control and to characterize the interaction between arrhythmias and conduction blocks.

2.4.1 Development of transgenic hiPSC lines

hiPSCs were transduced with lentivirus to express either ChR2 or *Gt*ACR2. YFP fluorescence following FACS demonstrates successful transduction of hiPSCs and transmembrane localization of the ChR2-YFP (**Figure 2.5A**) and *Gt*ACR2-YFP fusion proteins. Transgenic hiPSCs stained positive for Nanog, Sox2, and Oct3/4, confirming maintenance of pluripotency (**Figure 2.5A).**

2.4.2 Differentiation of light-sensitive cardiomyocytes

Transgenic hiPSCs were subsequently differentiated into light-responsive cardiomyocytes [81] (**Figure 2.5B**). Spot illumination of ChR2-expressing cardiomyocytes with 470nm light enabled spatially targeted depolarization and subsequent radial propagation of contractile activity (**Figure 2.5C**), while *Gt*ACR2-expressing cardiomyocytes stopped contracting when illuminated with 470nm light (**Figure 2.5D**).

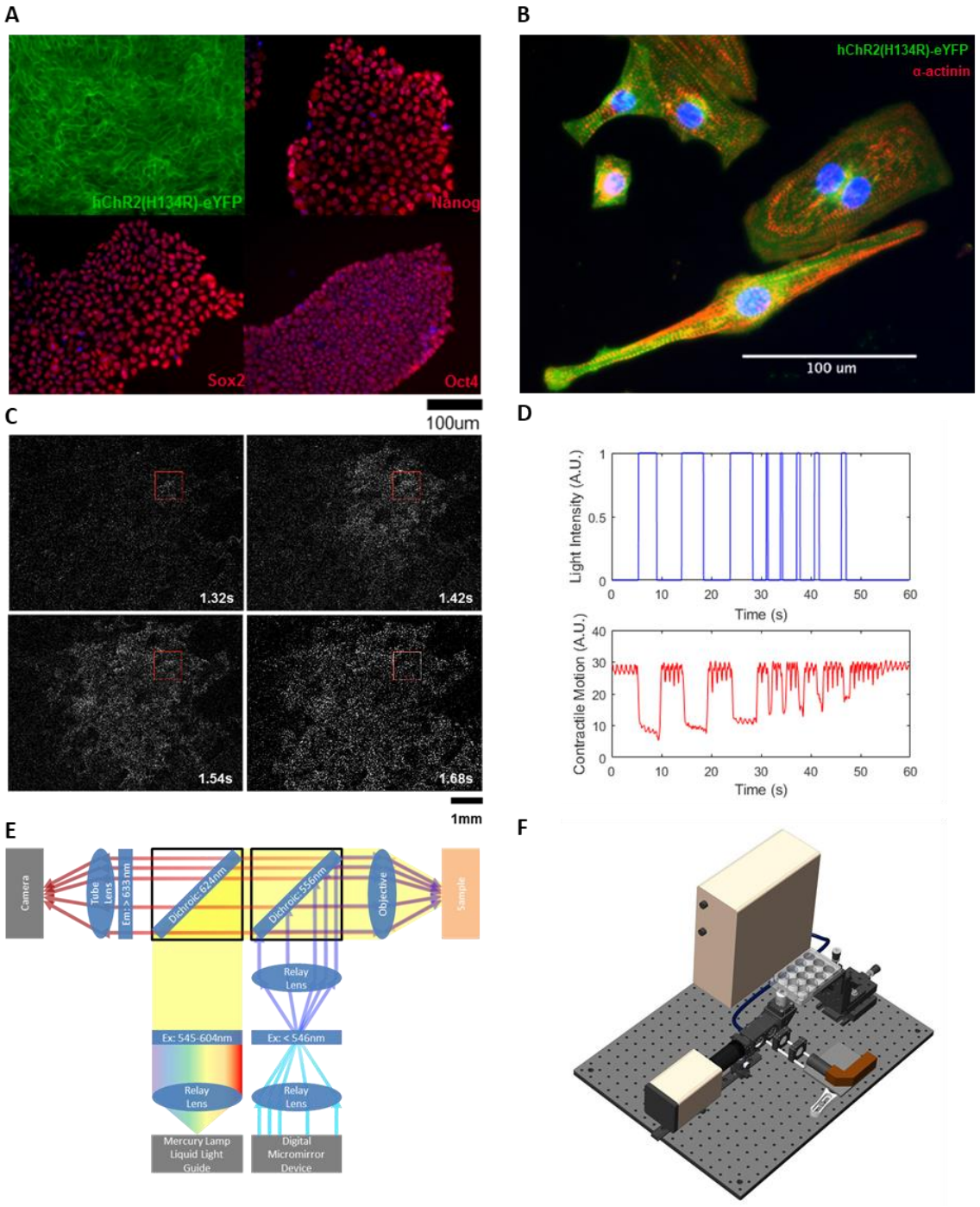

Figure 2.5: Creation of an in vitro platform for spatiotemporal control of human cardiac tissue through optogenetics

(A) Transmembrane localization of ChR2-eYFP fusion protein and maintenance of pluripotency markers in hiPSCs following transduction. **(B)** Transgenic hiPS-CMs stain positive for α-actinin. **(C)** Bright field imaging of ChR2-expressing hiPS-CM monolayers show single-spot illumination of the red square followed by radial propagation of contraction. Image processing is used to identify contractile motion (white pixels show motion). **(D)** GtACR2-expressing hiPS-CM monolayers cease contraction in response to illumination. **(E-F) D**iagram and solidworks rendering of the projector integrated into the optical mapping system.

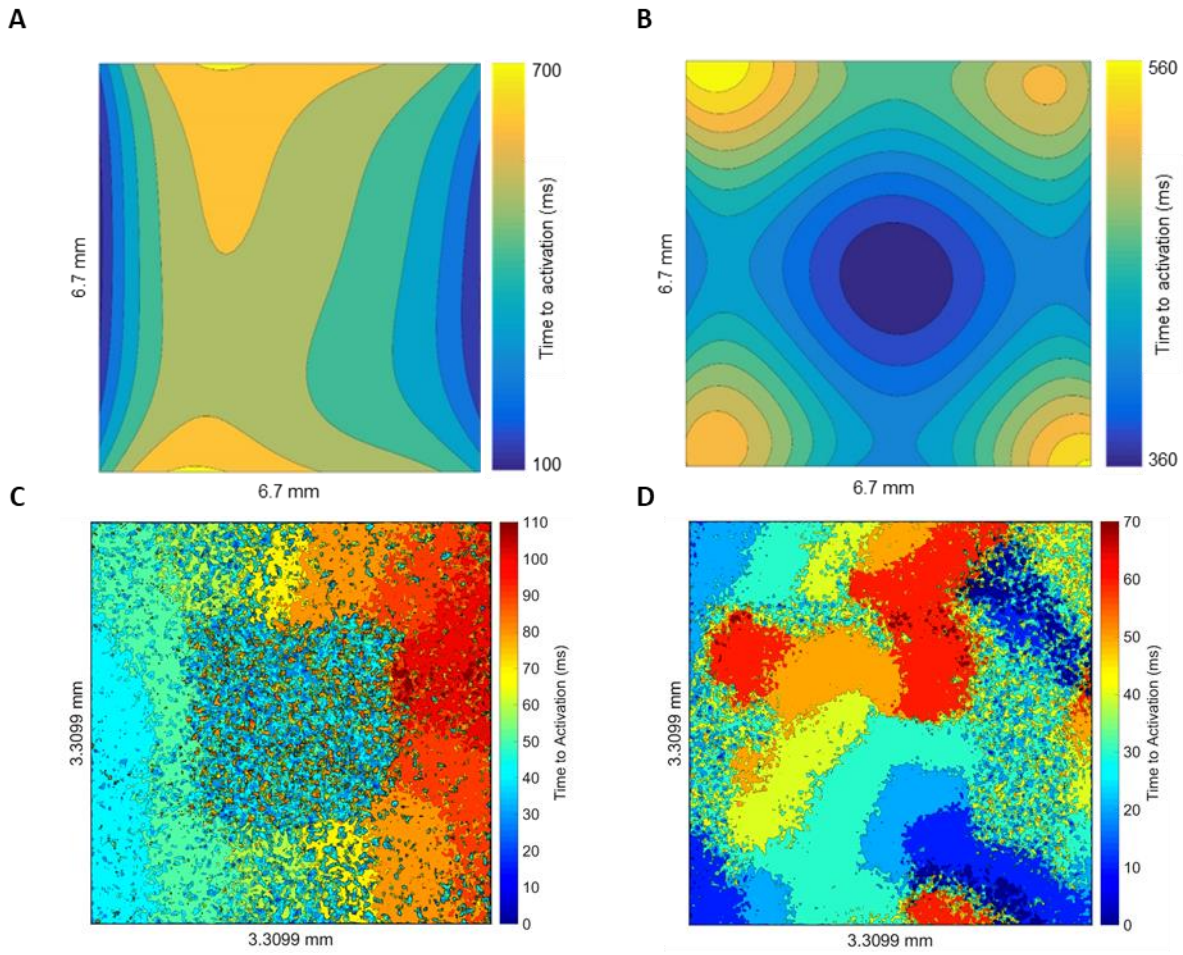

Figure 2.6 Spatiotemporal control of electrical activity through optogenetics.

Patterned illumination allow us to generate arbitrary waveforms in ChR2-expressing hiPS-CM monolayers such as (A) colliding waves and (B) a cross. Patterned

illumination allows us to generate arbitrary conduction blocks in GtACR2-expressing hiPS-CM monolayers such as (C) a square, and (D) the outline of a cat.

2.4.3 Development of a platform for simultaneous patterned illumination and optical mapping

In parallel, a projector was integrated into an optical mapping system for simultaneous patterned illumination and imaging (**Figure 2.5E-F**). A number of dyes were tested for compatibility with our optogenetic proteins. All optical mapping data was collected with the Cal-590 calcium dye, which was selected for its wavelength compatibility as well as for its stability for long duration imaging. Custom MATLAB software was developed to analyze the resulting videos.

2.4.4 Platform capabilities

Arbitrary illumination patterns such as a cross (**Figure 2.6A**) or two rectangles on opposite sides of the imaging area (**Figure 2.6B**) initiated wavefronts in ChR2-expressing monolayers that propagated into neighboring regions. In *Gt*ACR2-expressing monolayers, conduction was blocked in illuminated regions (**Figure 2.6C**), with more complex conduction blocks leading to more complex waveforms (**Figure 2.6D**).

2.5 Aims

The following aims were selected to demonstrate the breadth of research questions that can be answered using our system. To characterize the impact of anatomic defects with high precision, we utilized anion channelrhodopsin to generate light-inscribed conduction blocks, and dynamically modulate them to manipulate spiral waves in novel ways. We then tested spatially extended control schemes in heterogeneous monolayers of channelrhodopsin-expressing cardiomyocytes. Finally, we used hiPSCs from long QT patients to study the impact of prolonged action potential durations on spiral wave termination efficiency.[87,88]

Aim 1: Characterizing the interaction between reentry and conduction blocks

Aim 2: Spatiotemporal control of heterogeneous substrates

Aim 3: Defibrillating spiral waves in LQT8

3 AIM 1: CHARACTERIZING THE INTERACTION BETWEEN REENTRY AND CONDUCTION BLOCKS

3.1 Rationale

As previously discussed, reentry is more prevalent in the context of anatomic heterogeneities that lead to source-sink mismatches, wave break, and vortex shedding. The goals of this section are therefore two-fold. The first is to validate the use of light-inscribed conduction blocks to study the impact of anatomic heterogeneities on reentry. The second is to demonstrate its utility by addressing outstanding questions. All experiments involve the use of patterned illumination of *Gt*ACR2-expressing hiPS-CM monolayers to generate light-inscribed conduction blocks.

3.2 Results

3.2.1 Light-inscribed conduction blocks initiate and maintain reentry

To validate the use of light-inscribed conduction blocks, we sought to show that the interaction between propagating waves with light-inscribed conduction blocks could functionally replicate important behaviors attributed to anatomic heterogeneities.

3.2.1.1 Light-inscribed conduction blocks initiate functional reentry through vortex shedding

Anatomic heterogeneities are an important factor in the initiation of reentry through behaviors such as vortex shedding, whereby traveling waves interact with static conduction blocks to generate spiral waves.[20] Our light-inscribed conduction blocks recapitulate this behaviour (**Figure 3.1A)**, and can thus be used to study the physiologic phenomena underlying these interactions. In comparison with a rectangular block **(Figure 2.6C**), the wave must make a sharper turn to wrap completely around the arm of the backwards "C" used here while remaining adherent to the obstacle, thereby increasing the propensity for detachment and spiral wave formation.[20]

3.2.1.2 Functional reentry converts to anatomic reentry upon interaction with conduction blocks of the appropriate size

As our system allows us to dynamically modulate our conduction blocks, we use this capability to explore other phenomenon. For instance, slowly growing the size of our conduction blocks allow us to capture pre-existing spiral waves that are freely rotating in the monolayer, such that they adhere to the conduction block and start rotating around the conduction block (**Figure 3.1B**). It has been shown computationally that spiral waves are attracted to localized heterogeneity,[89] and experiments have also demonstrated the size-dependent capture effect shown here.[26]

3.2.2 Reentrant circuits pinned to light-inscribed conduction blocks can be moved

Furthermore, the spiral waves remain pinned to the conduction block even when the conduction block is moved (**Figure 3.1C**), allowing us to freely relocate spiral waves. This phenomenon can also be observed across large distances, such as when moving the monolayer itself. The ability to relocate spiral waves to desired locations greatly increases our capabilities for experiments such as the systematic study of spiral waves and their interaction with anatomic heterogeneities and each other.[27,90] It could also be used as a

means of controlled defibrillation through phase singularity-boundary collision, or phase singularity-phase singularity collision.[91]

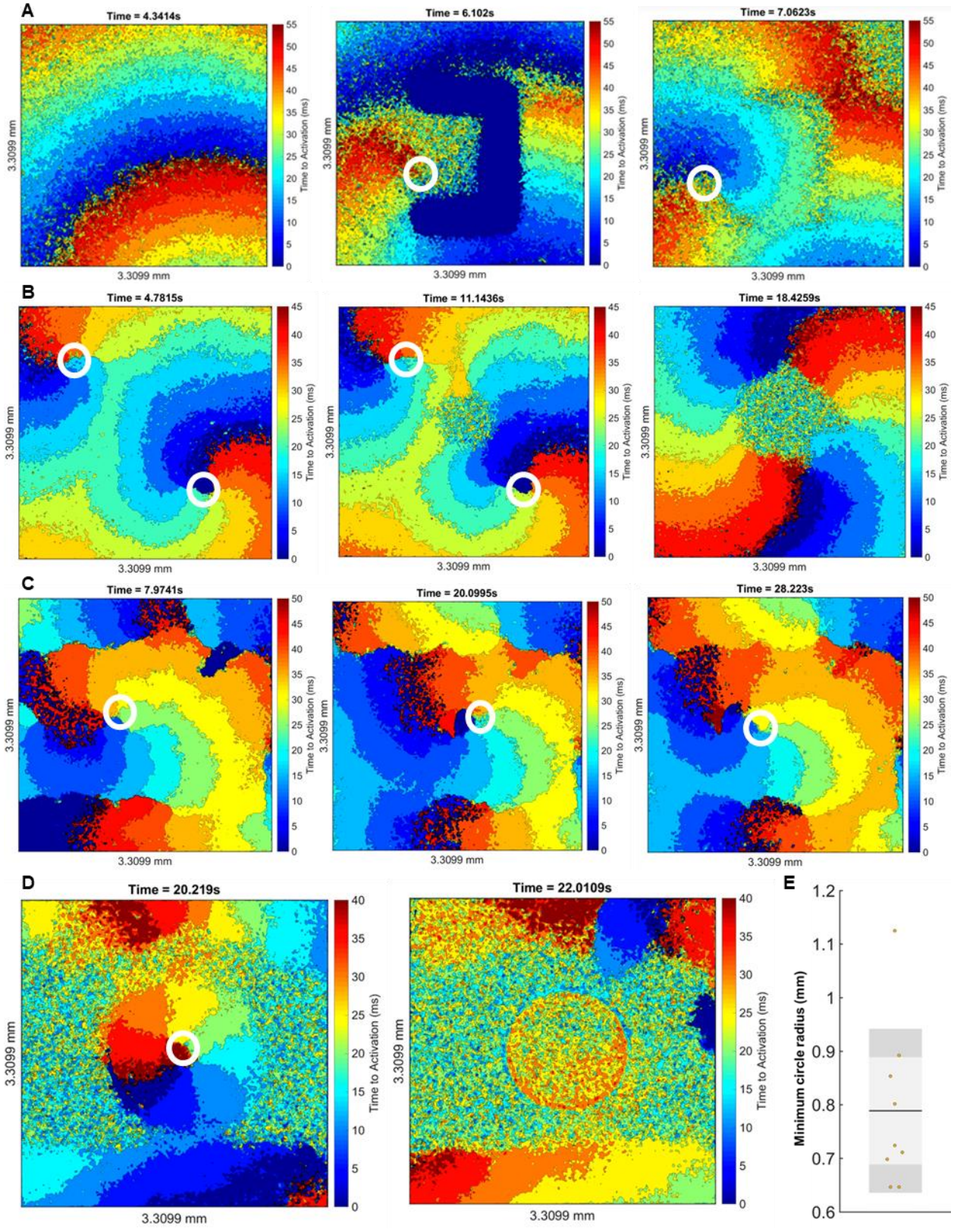

Figure 3.1 Dynamic light-controlled conduction blocks.

(A) Vortex shedding and the formation of a spiral wave. **(B)** Freely rotating spiral waves pin to an expanding light-generated conduction block. **(C)** A spiral wave is isolated inside a box inscribed by light, and pinned to a light-generated conduction block. The conduction block is then moved, first to the right, and then to the left, and the spiral wave follows. **(D)** A spiral wave is isolated inside a gradually shrinking circle until it dissipates. **(E)** Distribution of circle radii when the spiral wave dissipates (n = 9, mean +/- s.e.m. (light gray) and s.d. (dark gray)).

3.2.3 Gradually shrinking the electrically active substrate in the neighbourhood of functional reentry results in reentry termination below a critical size

Finally, we note that we are able to isolate spiral waves by using light to inscribe conduction blocks in a border around the phase singularity (**Figure 3.1C-D**), effectively isolating its domain from the rest of the monolayer. We realized that this would allow us to measure the minimum area of tissue capable of sustaining reentry, which is of interest in relation to the critical mass hypothesis [92–95]. We hypothesized that we could slowly shrink the borders around the phase singularity, and measure the radius of the resulting isolated monolayer when it dissipated (**Figure 3.1D**). We found that the average monolayer radius when the spiral wave dispersed was 0.79mm, with a minimum radius of 0.65mm (**Figure 3.1E**). We suggest that the corresponding minimum area of 1.33mm^2 is close to the smallest hiPS-CM monolayer that can support sustained reentry. This number is much smaller than the smallest area demonstrated for *in vivo*/*ex vivo* tissue, likely reflecting the lower conduction velocities in the hiPS-CM monolayer model as slower propagation speeds/shorter wavelengths enable reentry in smaller areas of tissue [94,96,97].

3.3 Discussion

In terms of functional validation, we have demonstrated that the illuminated regions exhibit classic behaviors associated with conduction blocks such as the initiation, maintenance, and termination of reentry.

Mechanistically, there is some additional nuance to the interpretation of the results. Technically, the boundary conditions for light-inscribed blocks involving the pinning of the

membrane voltage to a hyperpolarized stated, which decreases the source-sink ratio in the neighbourhood of the conduction block. This is different from conduction blocks with no-flux boundary conditions such as collagen scar or anatomic structures, which exert no effect on the source-sink ratio beyond the geometric considerations. Therefore, light-inscribed blocks should likely be considered more similar to anatomic heterogeneities involving cells such as damaged cardiomyocytes or fibroblasts that similarly lower the source-sink ratio in their neighbourhood. Clinically, the peri-infarct zone often includes a large proportion of nonmyocytes that couple with myocytes in the neighboring healthy tissue.[98,99] As such, the correct source-sink relationship at the boundary to model scar tissue likely varies on a case-by-case basis.

Further complicating the picture is that the effect of no-flux conduction blocks is size-dependent. As the size of the conduction block shrinks, anatomic reentry gradually transitions to functional reentry.[26] As previously described, functional reentry is characterized by a gradient of gradually decreasing source-sink ratio that terminates when that ratio reaches a critical point, leaving a nonexcited but excitable core region. Again, this is similar to what we have with light-inscribed conduction blocks. Finally, the effect of the boundary condition diminishes in importance away from the boundary, so the spatial scale of the experiment should be taken into account when determining its importance.

In terms of utility, it should be obvious that light-inscribed conduction blocks offer higher throughput than techniques which involve irreversible modification of the substrate such as manual excision. Further, the ability to dynamically alter our patterns allows us to perform experiments not previously possible, such as the relocation of spiral waves. Finally, the critical mass experiments demonstrate the increased technical capability offered by this system by smoothly varying parameters of interest until qualitative changes in behaviour occur.

4 AIM 2: SPATIOTEMPORAL CONTROL OF HETEROGENEOUS SUBSTRATES

4.1 Rationale

As previously discussed, in addition to the use of our platform to model conduction blocks, the other goal was to test spatially extended control schemes based on the hypothesis that this would be better than local pacing. Therefore, we would like to demonstrate qualitative improvements in our ability to control electrical activity through the use of spatially extended control schemes in comparison with local pacing using our platform. We hypothesized that the differences between local pacing and spatially extended control schemes would best be shown through the use of spatially heterogeneous substrates.

4.2 Results

4.2.1 Heterogeneous monolayers demonstrate disorganized waveforms

To generate a spatially heterogeneous substrate, ChR2-expressing hiPS-CMs were re-plated into heterogeneous clumps of cardiomyocytes, which were then connected by proliferating fibroblasts. This substrate exhibited highly disorganized spontaneous waveforms (**Figure 4.1A)**.

4.2.2 Qualitative restoration of planar wave propagation can be accomplished using dynamic pacing

Two types of control pulses were compared to restore traveling waves of electrical activity: (*i*) static pacing of the right half-plane, and (*ii*) dynamic traveling waves moving from right to left. Each control pulse was preceded by a full-field pulse to uniformly depolarize the monolayer. Static pacing of the right half-plane failed to restore the normal propagation of traveling waves through this substrate (**Figure 4.1B**). In contrast, the projection of propagating waves of light restored the normal propagation of cardiomyocyte depolarization (**Figure 4.1C**). This shows that the use of spatially extended control schemes can be qualitatively better than localized pacing schemes.

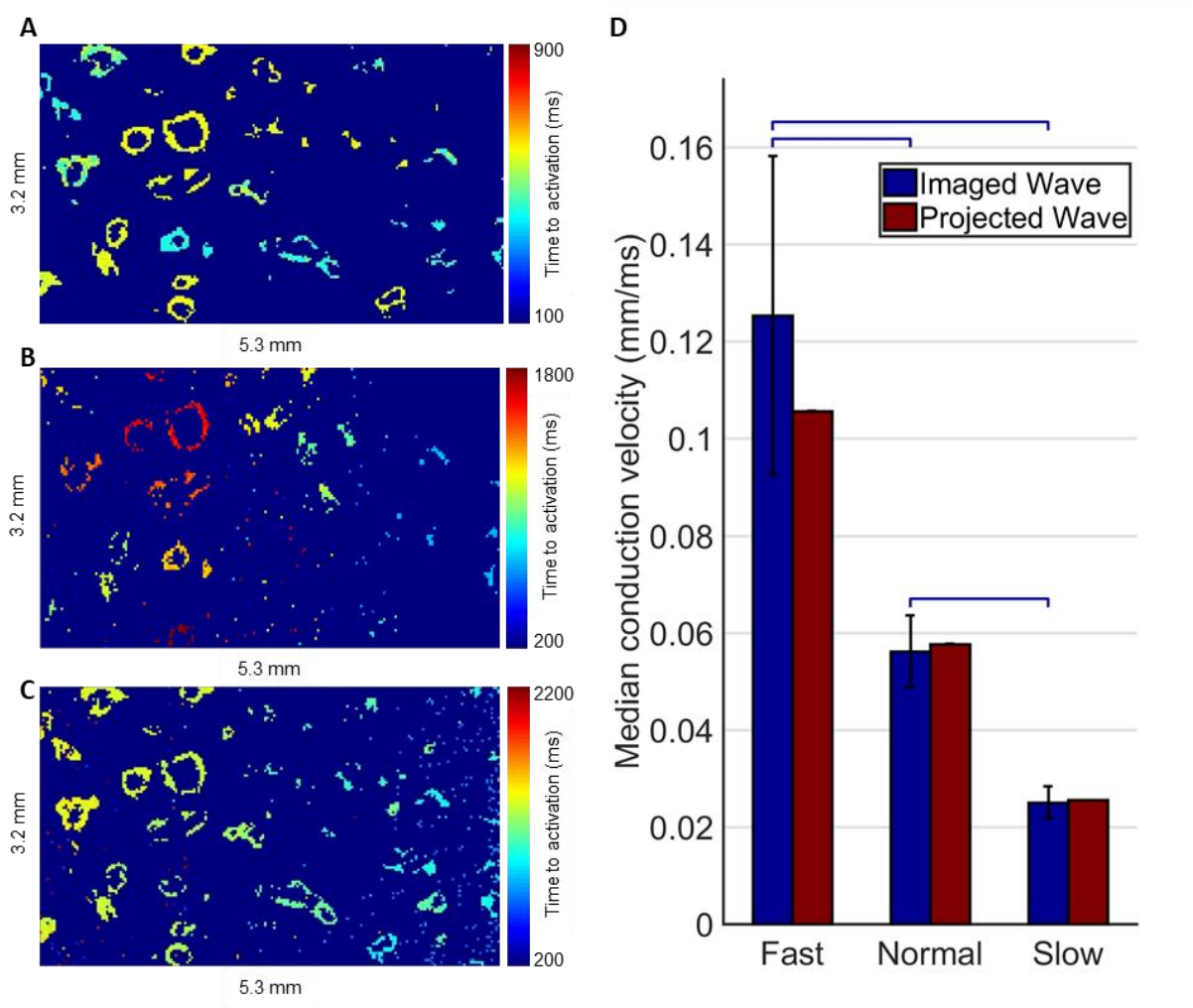

Figure 4.1 Dynamic light-controlled depolarization in heterogeneous monolayers

(A) Heterogeneous monolayers exhibit disorganized conduction. (B) Static pacing of the right half-plane failed to restore the orderly propagation of electrical activity. (C) Projection of traveling waves rescues orderly propagation of electrical activity as a planar wavefront. (D) The speed of imaged waves (blue bars) closely matched the speed of projected waves (red bars). (n >= 5 for each group, mean ± 95% confidence intervals, p < 0.05, two-sample t-test).

4.2.3 Quantitative control of wave propagation speed

Over a wide range of speeds, the speed of the imaged wave closely matches the speed of the projected wave (**Figure 4.1D**). This shows that our system is able to exert quantitative control over wave propagation in the underlying substrate.

4.3 Discussion

This study shows that in cases of anatomic heterogeneity, spatially extended control algorithms can succeed in controlling waveforms in cases where local pacing fails. This corroborates both computational[61] and clinical studies,[50] which show that an increased number of control points can achieve better control of electrical activity, and supports the further development of spatiotemporal control schemes. Further, based on these results, our platform appears to be suitable for high-throughput *in vitro* testing of control schemes.

One caveat to the results shown here is that our heterogeneous substrate does not exhibit classical reentry, likely due to the specific ratio of cardiomyocytes to fibroblasts and their seeding locations. Adopting doubly transduced cell lines expressing both depolarizing and hyperpolarizing optogenetic channels would allow us to simultaneously control both substrate geometry as well as the control sequence.

5 AIM 3: DEFIBRILLATING SPIRAL WAVES IN LQT8

5.1 Rationale

To further demonstrate the utility of hiPSCs in this system, patient-derived hiPSCs were used to model LQT8, where L-type calcium channel mutations interfere with channel inactivation, resulting in abnormal calcium overload and prolonged action potential.[87] The long-QT syndromes are important for a number of reasons. Clinically, untreated patients have a mortality rate of 21% within 1 year of the first syncopal episode, a statistic that decreases to 1% over 15 years with optimal management.[5] The strong genotype-phenotype correlation and wide range of mutations also makes LQTS one of the best models for studying mechanisms that predispose patients to arrhythmias and sudden cardiac death. We would like to use our system to study the effect of the LQT8 mutation on defibrillation success rates.

5.2 Results

5.2.1 A disease model of LQT8 using patient-derived hiPSCs.

Patient cell lines were transduced with ChR2, and differentiated into cardiomyocytes with extended action potential durations. Spiral waves spontaneously formed in the resulting monolayers.

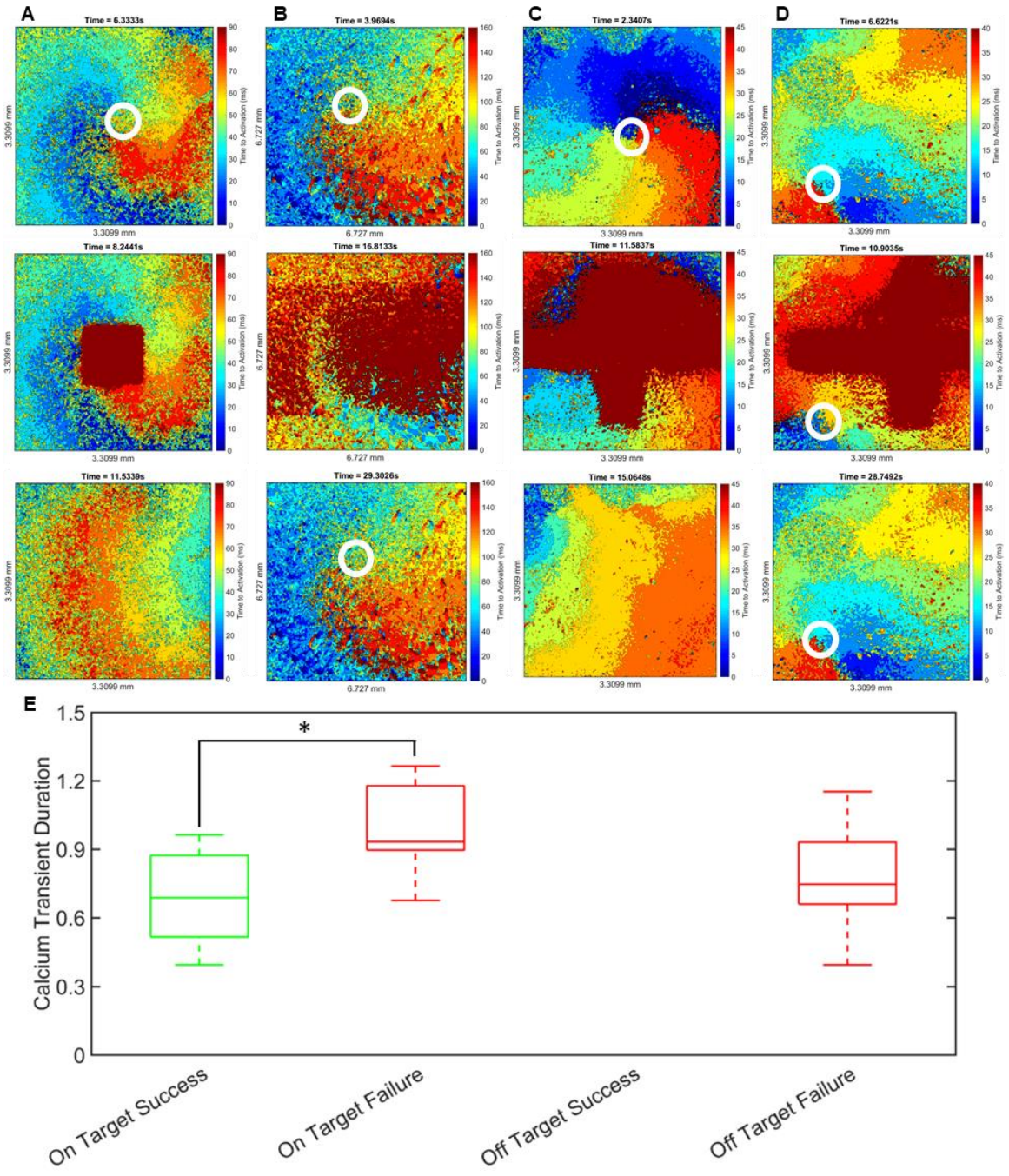

Figure 5.1 Spiral wave defibrillation in Timothy Syndrome monolayers.

(A) Successful defibrillation sequence in monolayer with calcium transient duration of 475ms. **(B)** Failed defibrillation sequence in monolayer with calcium transient duration of 1300ms. **(C)** Successful defibrillation sequence in monolayer with on-target defibrillation pulse. **(D)** Failed defibrillation sequence in monolayer with off-target defibrillation pulse. **(E)** Quantification of defibrillation results as a function of calcium transient duration and targeting (n = 189, mean +/- first and third quartile (box) and whole range (brackets), p = 2.267e-07 < 0.05, two-sample t-test).

5.2.2 Dependence of defibrillation success rate on calcium transient duration

We found that spiral waves with short calcium transients were easy to destabilize using 100-ms duration pulses of light and relatively small illumination areas (**Figure 5.1A**). However, spiral waves with long calcium transients were more difficult to destabilize, even using larger illumination areas (**Figure 5.1B**).

5.2.3 Dependence of defibrillation success rate on location of defibrillatory impulse

We also explored the relationship between illumination pattern and spiral wave defibrillation. An illustrative example shows that illumination of the spiral wave core for a spiral wave pinned to anatomic heterogeneities leads to successful unpinning (**Figure 5.1C**), whereas failure to illuminate the spiral wave core for a second spiral pinned to the same location leads to failed defibrillation (**Figure 5.1D**).

5.2.4 Quantification

To summarize these findings, over the course of 189 defibrillation attempts (117 attempts with on-target defibrillation, 72 attempts with off-target defibrillation) using a variety of illumination geometries, we can see that there were no instances of successful defibrillation when the illuminated region missed the phase singularity (**Figure 5.1E**). Further, the average calcium transient duration for successful defibrillation attempts was significantly shorter than that for failed defibrillation attempts (**Figure 5.1E**), indicating that the increase in action potential duration also increases the resistance of individual rotors to termination secondary to external pacing.

5.3 Discussion

While these results seem biologically plausible given the increased arrhythmogenicity associated with the long-QT syndromes, it contrasts with a previous study in Langendorff-perfused rat hearts where pharmacologically shortened action potential durations prevented arrhythmia termination following a single 1s long optogenetic impulse.[100] Further studies will be required to tease apart the differences in geometry, electrophysiology, and defibrillation strategy between these two studies using different species.

6 DISCUSSION AND FUTURE WORK

6.1 Technical advances

The work described here demonstrates a number of technical advances compared to the existing literature. In particular, this is the first study to generate stable optogenetic hiPSC lines, to look at patterned illumination in optogenetic human cardiac substrates, and to use anion channel rhodopsins to generate light-inscribed conduction blocks in cardiac tissue.

6.1.1 Patterned illumination of optogenetic human cardiac substrates

In the intervening time since this project was conceived, patterned illumination of optogenetic substrates was used for the *in vitro* control of electrical activity in animal cardiac cells and tissues.[69,101,102] However, despite the successful genetic engineering of hiPS-CMs to express channelrhodopsin following differentiation, those studies did not extend to the application of patterned illumination.[103] This is therefore the first instance of patterned illumination of optogenetic human cardiac substrates. The use of stable transgenic human stem cell lines allows for experimentation in human models with human electrophysiology, and also obviates the need for repeated genetic modification for each experiment using primary cells.

The generation of stable optogenetic hiPSC lines and their differentiation into cardiomyocytes allowed for consistent experimentation in human substrates with human

electrophysiology, and also obviates the need for repeated genetic modification for each experiment using primary cells. To further illustrate the utility of hiPSC technology, we additionally conducted studies using patient-specific cells, demonstrating the potential for personalized genetic disease models.

6.1.2 Patterned illumination of hyperpolarizing optogenetic channels for light-inscribed conduction blocks

In contrast to previous reports in animal substrates,[102] continuous illumination of ChR2-expressing hiPS-CMs rarely generated conduction blocks. Further, the initial illumination of ChR2-expressing cardiomyocytes generated a depolarization wavefront that disrupted the existing waveforms, a known phenomenon that limits the applicability of this technique. As such, the introduction of hyperpolarizing optogenetic channels to generate light-inscribed conduction blocks represents a major technical advance in our ability to generate spatially heterogeneous substrates. The ability to dynamically manipulate conduction blocks in real-time represents a novel and powerful tool for the study of spiral wave dynamics in spatially heterogeneous substrates, particularly through the ability to reproducibly relocate spiral waves to desired locations.

6.2 Scientific findings

New scientific findings described in this dissertation include the ability to model anatomic heterogeneities using light-inscribed conduction blocks, the superiority of spatially extended control schemes to control arrhythmias in spatially heterogeneous models, and the detrimental impact of prolonged APD on spiral wave defibrillation efficiency using single pulses of light.

6.2.1 Light-inscribed conduction blocks using hyperpolarizing optogenetic proteins recapitulate key behaviors of anatomic heterogeneities

The coupling of patterned illumination and hyperpolarizing optogenetic tools allowed us to generate dynamic, light-inscribed conduction blocks, and to observe spiral wave formation, pinning, and termination at a critical minimum area. These behaviors are consistent with the effects of anatomic heterogeneities generated using other means, and confirm the utility of our system in studying these interactions.

6.2.2 Important parameters in our system are related to the wavelength

The critical minimum area capable of supporting reentry in hiPS-CM monolayers has not been previously measured. The value that we measured was substantially smaller than that found in native tissue. Similarly, the obstacles to which spiral waves adhered in our system were also quite small. Both parameters are closely related to the conduction velocity and reentry wavelength,[26] and the small values found in our system are consistent with the decreased conduction velocities and wavelengths found in hiPS-CM monolayer preparations.

6.2.3 Spatially extended control schemes are superior to local pacing schemes in spatially heterogeneous models

Using monolayers of optogenetic human cardiomyocytes, we showed that spatially extended control schemes are necessary to achieve control in heterogeneous substrates, in line with computational results.[61] Clinically, this suggests that current pacing methods that rely on a small handful of electrodes are likely insufficient to control the propagation of electrical activity in patients with extensive regions of anatomic heterogeneity. The substrate used here is reminiscent of the peri-infarct zone following myocardial infarctions, which is characterized by bundles of viable cardiomyocytes separated by scar tissue. In patients with scar tissue, it was shown that the use of multiple point pacing led to better outcomes compared to single point pacing.[50] Our results are complementary, and together support the continued development of flexible electronics, which could theoretically offer hundreds of control points.[52]

6.2.4 Prolonged action potential durations associated with long QT syndrome decrease defibrillation efficiency

Our studies of monolayers derived from patients with long QT syndrome showed that the prolonged action potential durations in these patients decrease the success rate of spiral wave termination by exogenous pacing. In combination with previous results,[100] this suggests that the relationship between action potential duration and ease of spiral wave termination is nonlinear in nature. It was previously shown that pharmacological lengthening of the action potential duration decreased the average number of rotors.[91] The decrease in the average number of rotors previously documented means that each individual rotor exerts its influence over a larger domain, thereby decreasing the probability of rotor termination through

collision with wavefronts generated by neighboring rotors and potentially accounting for part of the observed increase in rotor stability.

6.3 Limitations

6.3.1 Shortcomings of the hiPS-CM monolayer model

There are a number of shortcomings for the hiPS-CM monolayer model when it comes to modelling real human cardiac tissue, primarily related to maturation. The immaturity of these cells means that important electrophysiological properties such as conduction velocity are much lower in monolayers. These deficiencies are currently being addressed in *in vitro* tissue engineered models.[104]

6.3.2 Characterization of light-inscribed conduction blocks

An additional aspect that needs further characterization is the nature of light-inscribed conduction blocks, and how similar they are to conduction blocks caused by myocardial infarction. In particular, the light-activated anion channels drive down the membrane potential whereas myocardial infarction is traditionally thought to create no-flux boundary conditions. However, recent studies have challenged this notion, and have suggested that heterocellular electrotonic coupling occurs between nonmyocytes and cardiomyocytes following scar formation.[99] A direct comparison is warranted to further clarify the suitability of light-inscribed conduction blocks as a model of infarction.

6.4 Future directions: Bridging gaps in translation

Our platform is located at the intersection of four rapidly innovating fields: computational modeling, cell and tissue engineering, optogenetics, and personalized medicine. This platform draws on a number of technologies from these disciplines to evaluate hypotheses, and bridge the gap between computational models and clinical translation in the field of arrhythmogenesis and control (**Figure 6.1**).

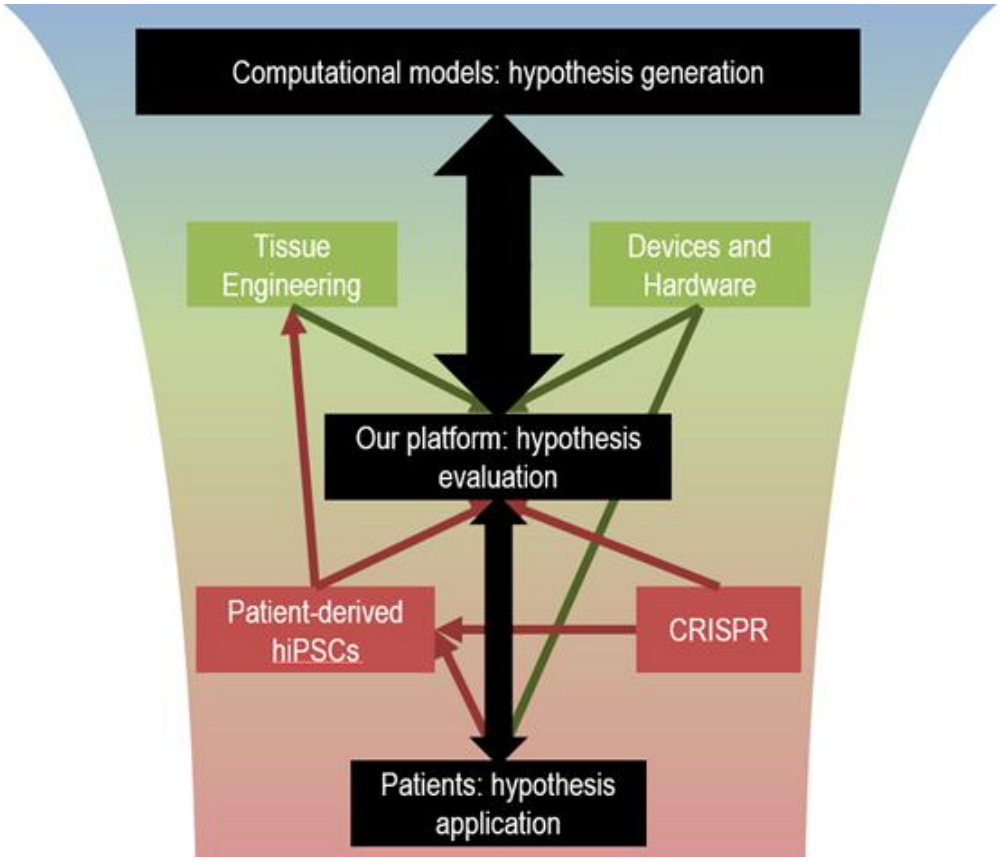

Figure 6.1: Contextualizing our platform

With appropriate validation, the ability to generate light-inscribed conduction blocks that recapitulate the interaction between anatomic heterogeneities and spiral wave behavior opens the door for the high-throughput testing and prediction of arrhythmia risk as a function of patient scar geometry, as well as the performance of virtual catheter ablations.

Further genetic engineering to create doubly transduced cell lines and mouse models would allow for additional exploration. Clinical mapping data could be used in conjunction with computational models and our platform to determine the optimal electrode placement and defibrillation patterns with respect to scar tissue and other conduction blocks (**Figure 6.2**).

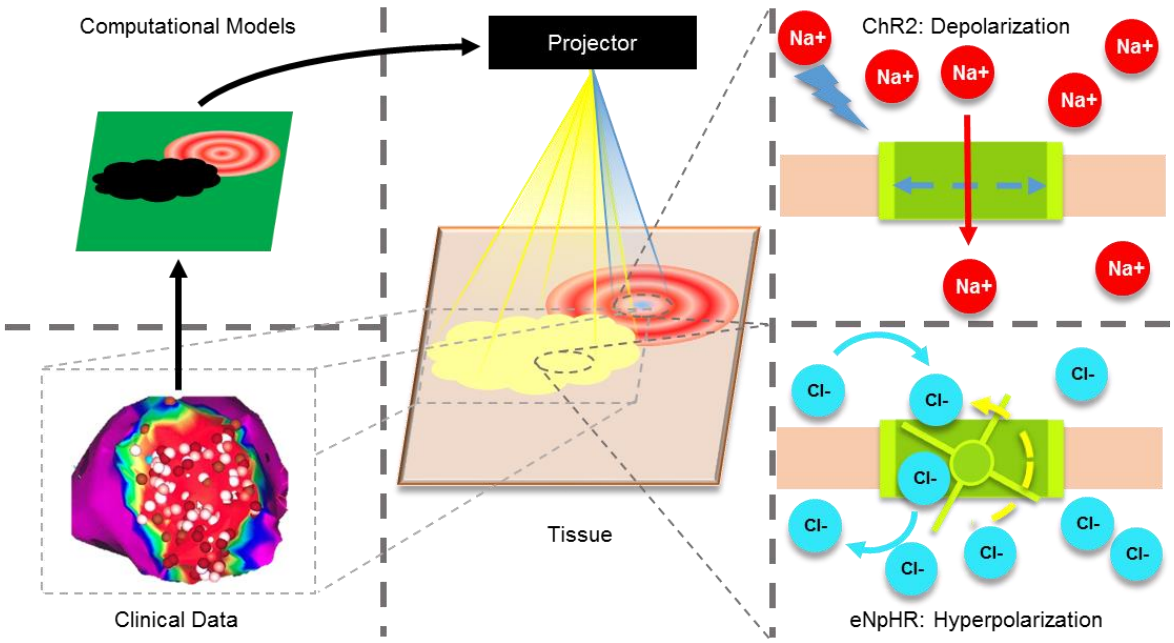

Figure 6.2 Modeling patient scar tissue and defibrillation strategies

6.5 Concluding thoughts

In summary, the optogenetic approach described here allows for precise spatiotemporal modulation of electrical activity in human cardiac tissue, with direct translation to clinical applications. With advancements in cardiac tissue engineering and further genetic engineering to generate doubly transduced optogenetic cell lines, we foresee high-throughput optimization of electrode placement and defibrillation algorithms for personalized anatomic and functional defects. The combination of patterned conduction blocks, patient-derived cells, and spatially extended control schemes thus forms a basis for personalized disease models and interventions.

7 MATERIALS AND METHODS

7.1 Stem cell culture

Experiments on healthy stem cells were performed using C2a[105] and WTC-11 (from the Bruce Conklin laboratory) hiPSCs . Timothy Syndrome experiments were performed using T-3-5 hiPSCs.[88] Stem cells were maintained in mTeSR™1 (Stemcell Technologies #85850) + 1% v/v penicillin/streptomycin (ThermoFisher Scientific #12430-047). Media was changed daily for three to four days between passages. For passaging, standard 6-well tissue culture plates were pre-coated for stem cell culture with 1mL/well of Matrigel (ThermoFisher Scientific #CB-40230) diluted in DMEM/F12 (ThermoFisher Scientific #11320-033) at a ratio of 1:80. Plates were stored at 4°C for up to two weeks before culture. Prior to passaging, plates were incubated at room temperature for one to four hours. Stem cells were dissociated by incubation with 0.5mM EDTA (ThermoFisher Scientific #15575-038) in PBS (ThermoFisher Scientific #21-040-CV)for five minutes followed by rigorous mechanical shearing with a P1000 pipette. Stem cells were seeded at a ratio of 1:12 in mTeSR™1 + 2µM Y-27632 dihydrochloride (Tocris 1254) in 2mLs total volume per well.

7.2 Lentiviral transduction

Transgenic cell lines were created by infection of hiPSC lines with lentivirus. For ChR2-expressing cell lines, we used the commercially available pLenti-EF1a-hChR2(H134R)-EYFP-WPRE (Addgene #20942, [106]) plasmid. For hyperpolarizing cell lines, the *Gt*ACR2 sequence was cloned from a commercially available plasmid (pFUGW-hGtACR2-EYFP ,

Addgene #67877, [71]) into the pWPXL backbone (Addgene #12257) for subsequent transduction into hiPSCs. The EF1α promoter was chosen to ensure expression of the ChR2-YFP/GtACR2-YFP fusion proteins in both stem cells (for selection by FACS) and their differentiation products (for optical stimulation). After infection, YFP+ cells were selected by FACS and expanded to create transgenic cell lines.

Human embryonic kidney cells HEK-293FT (ThermoFisher Scientific # R700-07) grown in Dulbecco's Modified Eagle Media (ThermoFisher Scientific #11965-092) supplemented with 2% v/v of fetal bovine serum (FBS) (Atlanta Biologicals #S11150) and 1% v/v penicillin/streptomycin (ThermoFisher Scientific #12430-047) were transfected with 32.73 µg of the target plasmid, 10.91 µg of viral envelope plasmid (pMD-gVSV-G) and 21.82 µg of packaging construct (pCMV ΔR 8.2) using polyethylenimine (Polysciences # 23966). After 60 hours supernatant was filtered through a 0.45 mm low protein-binding Steriflip-HV, (Millpore # SE1M003M00) and the viral particles were precipitated using Lenti-X Concentrator (Takara # 631231). Following transduction, YFP+ cells were selected by FACS and expanded.

7.3 Cardiomyocyte differentiation

Cardiomyocytes were differentiated following established protocols [107]. Briefly, differentiations were started when stem cells reached 70-90% confluence. The basal media for the differentiation sequence was CDM3, consisting of RPMI-1640 (ThermoFisher Scientific #11875-093) + 500ug/mL albumin (ScienCell OsrHSA) + 213ug/mL ascorbic acid (Wako chemicals 321-44823). On day 0, stem cells were incubated in CDM3 + 3-6uM CHIR (Tocris # 4423). On day 2, media was changed to CDM3 + 2uM Wnt-C59 (Tocris #5148). On day 4, media was changed to CDM3 with no supplements. Media was changed every two days afterwards. Cardiomyocytes commenced spontaneous beating between days 8-12, whereupon media was switched to RPMI + B27 (ThermoFisher Scientific #17504-044) + 213ug/mL ascorbic acid.

7.4 Brightfield contractility analysis

For movies S1 and S2, brightfield movies were processed to extract motion by subtracting every frame from a baseline frame to get a matrix of differences. The absolute value of the difference was visualized as an intensity image to display side-by-side with the original frame

in the movies. The amount of motion in each region of interest at any time point was calculated as the average absolute value of the difference matrix across the region of interest. This value was calculated for all time points to create the trace of contractile activity for each region of interest. The light intensity trace was extracted from the video by finding the average intensity value across the illuminated region for each time point. This value was thresholded to create a binary on/off trace to better represent the actual illumination sequence which was also a binary on/off sequence.

7.5 Optical platform for simultaneous patterned illumination and optical mapping

We selected the Andor Zyla 4.2 sCMOS camera for optical mapping due to its high spatiotemporal resolution (2048x2048 at 100fps), quantum efficiency, and signal-to-noise ratio at low light levels. The setup includes the camera, the tube lens (Edmund Optics #89-606, #89-905, #86-835), the imaging objectives (standard Olympus microscope objectives at varying magnifications), the relay lens system and dichroic mirrors used to couple the projector/digital micromirror device (Texas Instruments DLPLCR4500EVM) and mercury lamp (Nikon Intensilight C-HGFI) to the main light path, and the excitation/emission filters for channelrhodopsin and the calcium dye. This platform was used to simultaneously perform patterned illumination of optogenetic cardiac monolayers and high-speed optical mapping. All experiments were performed with maximum illumination intesntiy, ~1mW/mm^2.

7.6 Optical mapping

The calcium dye Cal-590^{TM} AM (AAT Bioquest #20510) was selected for its wavelength compatibility and its stability in long duration imaging. Cells were incubated in cardiomyocyte media containing 2mM Cal-590^{TM} AM with PowerLoad^{TM} (Thermofisher Scientific #P10020) at 37C for one hour. The incubation media was replaced with fresh cardiomyocyte media immediately prior to imaging.

7.7 Optical mapping analysis

Optical mapping analysis was performed using standard image processing techniques. Movies were preprocessed for optical mapping to reduce noise by spatial binning to a final

spatial resolution of 256x256 pixels, and by filtering every pixel with a low-pass frequency filter. Temporal windows for activation mapping were selected based on the interval between successive depolarizations in the monolayer (determined by the pacing frequency for paced videos, or spontaneous depolarizations/spiral wave activity in unpaced videos). Activation times were determined as either the time of maximum fluorescence intensity (F_{max}) or the time of maximum rate in fluorescence increase (dF/dt_{max}).

7.8 Light-inscribed conduction blocks (**Figure 3.1**)

Movies to project were generated using either Matlab or powerpoint. For experiments to study the initiation of spiral waves such as that shown in **Figure 3.1A,** regions with planar wave propagation were chosen for experimentation. For experiments manipulating spiral waves such as those shown in **Figure 3.1B-D**, pre-existing spiral waves were identified in the monolayer. The locations were manually centered, recording was commenced, and then the patterned illumination movies were started.

7.9 Spiral wave radius calculations (**Figure 3.1D-E**)

A rectangle with a hollow center circle was projected onto spiral waves in the monolayer. The radius of the hollow circle was gradually decreased until it disappeared. The behavior of the spiral wave was observed until it disappeared. The frame at which the spiral wave disappeared was manually selected in post-processing. A circle was then fitted to the image of the hollow circle using Matlab to determine its radius in that instant.

7.10 Creation of heterogeneous monolayers (**Figure 4.1**)

To generate a spatially heterogeneous substrate, ChR2-expressing hiPS-CMs differentiated following the above protocol were incompletely dissociated with a combination of collagenase digestion (Worthington LS004176, 2mg/mL in HBSS) and mechanical shearing using P1000 pipettes. Digestion times and amount of mechanical shearing were titrated on a well-by-well basis to achieve incomplete dissociation. Digestion products were centrifuged at 170 rcf for five minutes. Digestion products were resuspended in RPMI + B27 + 20% FBS, and then centrifuged again. Digestion products were again resuspended in RPMI + B27 + 20% FBS and then seeded at multiple concentrations. Wells for experimentation were chosen on the basis of heterogeneity. Experiments were performed one week after seeding, at

which point the clumps of cardiomyocytes were connected by a sheet of proliferating supporting cells.

7.11 Analysis of heterogeneous monolayers (**Figure 4.1**)

For heterogeneous monolayers, we needed to segment out the cardiomyocytes from the intervening supporting cells. Operating on the theory that cardiomyocytes and supporting cells have distinctly different fluorescent traces when imaged with calcium dyes, the intensity traces for each pixel were scored based on the fluorescence trace (e.g. maximum change in fluorescence) and automatically segmented into cardiomyocyte pixels vs. supporting cell pixels using k-means clustering or Otsu's method. This mask was used to select pixels for subsequent activation mapping. Polynomial fitting was then used to interpolate the gaps between the cardiomyocytes to generate smooth wavefronts. The gradient of this surface was calculated (dt/dDistance) and inverted to calculate conduction velocities at every point of the surface (dDistance/dt). The median conduction velocity was reported.

7.12 Timothy Syndrome spiral wave defibrillation quantification (**Figure 5.1**)

Spontaneously occurring spiral waves were identified, and various light patterns were projected onto the spiral waves to attempt defibrillation. In post-processing, defibrillation attempts were divided based on two criteria: 1) successful vs failed defibrillation attempts, and 2) patterns that illuminated the spiral centers vs patterns that failed to illuminate the spiral centers.

The calcium transient duration was calculated from the movies in post-processing. For each movie, the average calcium fluorescence trace for a 0.5mm x 0.5mm region at the border of the frame (away from the center of the spiral) was extracted. Criteria for minimum peak width/height were used to separate actual calcium transients from background noise in each fluorescence trace. The beginning and end of each transient was marked as the time at which the fluorescence intensity rose or fell to 10% of the full transient height. The calcium transient duration was calculated as the difference between these two times for each transient. An average calcium transient duration was calculated across at least five calcium transients occurring before defibrillation attempts started.

7.13 Statistical methods

Two-sample t-tests were used to compute p-values for **Figure 4.1D** and **Figure 5.1E**, and a statistical significance threshold of 0.05 was used to determine significance.

REFERENCES

1. Heron, M. Deaths: leading causes for 2010. *Natl. Vital Stat. Rep.* **62,** 1–96 (2013).

2. Zheng, Z. J., Croft, J. B., Giles, W. H. & Mensah, G. A. Sudden cardiac death in the United States, 1989 to 1998. *Circulation* **104,** 2158–63 (2001).

3. Ashikaga, H. *et al.* Magnetic resonance-based anatomical analysis of scar-related ventricular tachycardia: implications for catheter ablation. *Circ. Res.* **101,** 939–47 (2007).

4. Moss, A. J. *et al.* Long QT syndrome: from channels to cardiac arrhythmias. *J. Clin. Invest.* **115,** 2018–2024 (2005).

5. Schwartz, P. J., Crotti, L. & Insolia, R. Long-QT syndrome: from genetics to management. *Circ. Arrhythm. Electrophysiol.* **5,** 868–77 (2012).

6. McWilliam, J. A. Fibrillar Contraction of the Heart. *J. Physiol.* **8,** 296–310 (1887).

7. Mayer, A. G. *Rhythmical Pulsation in Scyphomedusae*. *Carnegie Institute of Washington* (1906). doi:10.5962/bhl.title.31914

8. Mines GR. On circulating excitations in heart muscle and their possible relation to tachycardia and fibrillation. *Trans. Proc. R. Soc. Canada* 43–52 (1914).

9. Gough, W. B., Mehra, R., Restivo, M., Zeiler, R. H. & el-Sherif, N. Reentrant ventricular arrhythmias in the late myocardial infarction period in the dog. 13. Correlation of activation and refractory maps. *Circ. Res.* **57,** 432–42 (1985).

10. Allessie, M. A., Bonke, F. I. & Schopman, F. J. Circus movement in rabbit atrial muscle as a mechanism of trachycardia. *Circ. Res.* **33,** 54–62 (1973).

11. Garrey, W. E. Auricular Fibrillation. *Physiol. Rev.* **4,** 215–250 (1924).

12. Allessie, M. A., Bonke, F. I. & Schopman, F. J. Circus movement in rabbit atrial muscle as a mechanism of tachycardia. III. The 'leading circle' concept: a new model of circus movement in cardiac tissue without the involvement of an anatomical obstacle. *Circ. Res.* **41,** 9–18 (1977).

13. Winfree, A. T. Spiral waves of chemical activity. *Science* **175,** 634–6 (1972).

14. Nattel, S., Xiong, F. & Aguilar, M. Demystifying rotors and their place in clinical translation of atrial fibrillation mechanisms. *Nat. Rev. Cardiol.* **14,** 509–520 (2017).

15. Cellular Basis for Cardiac Arrhythmias. Available at: http://tmedweb.tulane.edu/pharmwiki/doku.php/cellular_basis_for_arrhythmias?do=. (Accessed: 5th December 2017)

16. Hume, J. R. & Grant, A. O. in *Basic & Clinical Pharmacology, 13e* (eds. Katzung, B. G. & Trevor, A. J.) (McGraw-Hill Medical, 2015).

17. Pappone, C. *et al.* Wolff-Parkinson-White syndrome in the era of catheter ablation: insights from a registry study of 2169 patients. *Circulation* **130,** 811–9 (2014).

18. Pitt-Francis, J. *et al.* Chaste: A test-driven approach to software development for biological modelling. *Comput. Phys. Commun.* **180,** 2452–2471 (2009).

19. Frazier, D. W. *et al.* Stimulus-induced critical point. Mechanism for electrical initiation of reentry in normal canine myocardium. *J. Clin. Invest.* **83,** 1039–1052 (1989).

20. Cabo, C. *et al.* Vortex shedding as a precursor of turbulent electrical activity in cardiac muscle. *Biophys. J.* **70,** 1105–11 (1996).

21. Pandit, S. V & Jalife, J. Rotors and the dynamics of cardiac fibrillation. *Circ. Res.* **112,** 849–62 (2013).

22. Jalife, J. Experimental and clinical AF mechanisms: bridging the divide. *J. Interv. Card. Electrophysiol.* **9,** 85–92 (2003).

23. Gray, R. A. *et al.* Mechanisms of cardiac fibrillation. *Science* **270,** 1222-3; author reply 1224-5 (1995).

24. Ikeda, T. *et al.* Mechanism of spontaneous termination of functional reentry in isolated canine right atrium. Evidence for the presence of an excitable but nonexcited core. *Circulation* **94,** 1962–73 (1996).

25. Bingen, B. O. *et al.* Light-induced termination of spiral wave arrhythmias by optogenetic engineering of atrial cardiomyocytes. *Cardiovasc. Res.* cvu179- (2014). doi:10.1093/cvr/cvu179

26. Lim, Z. Y., Maskara, B., Aguel, F., Emokpae, R. & Tung, L. Spiral Wave Attachment to Millimeter-Sized Obstacles. *Circulation* **114,** 2113–2121 (2006).

27. Ikeda, T. *et al.* Attachment of meandering reentrant wave fronts to anatomic obstacles in the atrium. Role of the obstacle size. *Circ. Res.* **81,** 753–64 (1997).

28. Acosta, J. *et al.* Scar Characterization to Predict Life-Threatening Arrhythmic Events and Sudden Cardiac Death in Patients With Cardiac Resynchronization Therapy. *JACC Cardiovasc. Imaging* (2017). doi:10.1016/j.jcmg.2017.04.021

29. Demirel, F. *et al.* Myocardial scar characteristics based on cardiac magnetic resonance imaging is associated with ventricular tachyarrhythmia in patients with ischemic cardiomyopathy. *Int. J. Cardiol.* **177,** 392–399 (2014).

30. Yan, A. T. *et al.* Characterization of the Peri-Infarct Zone by Contrast-Enhanced Cardiac Magnetic Resonance Imaging Is a Powerful Predictor of Post-Myocardial Infarction Mortality. *Circulation* **114,** 32–39 (2006).

31. Kwon, D. H. *et al.* Infarct Characterization and Quantification by Delayed Enhancement Cardiac Magnetic Resonance Imaging Is a Powerful Independent and

Incremental Predictor of Mortality in Patients With Advanced Ischemic Cardiomyopathy. *Circ. Cardiovasc. Imaging* **7,** 796–804 (2014).

32. Nazarian, S. *et al.* Magnetic Resonance Assessment of the Substrate for Inducible Ventricular Tachycardia in Nonischemic Cardiomyopathy. *Circulation* **112,** 2821–2825 (2005).

33. Arenal, A. *et al.* Do the spatial characteristics of myocardial scar tissue determine the risk of ventricular arrhythmias? *Cardiovasc. Res.* **94,** 324–332 (2012).

34. Sonoda, K. *et al.* Scar characteristics derived from two- and three-dimensional reconstructions of cardiac contrast-enhanced magnetic resonance images: Relationship to ventricular tachycardia inducibility and ablation success. *J. Arrhythmia* **33,** 447–454 (2017).

35. Kalifa, J. & Avula, U. M. R. Ablation of Driver Domains During Persistent Atrial Fibrillation: A Call for More Understanding. *Circulation* **130,** 525–527 (2014).

36. Haissaguerre, M. *et al.* Driver domains in persistent atrial fibrillation. *Circulation* **130,** 530–8 (2014).

37. Shin, S.-H. *et al.* Mechanical dyssynchrony after myocardial infarction in patients with left ventricular dysfunction, heart failure, or both. *Circulation* **121,** 1096–103 (2010).

38. Keldermann, R. H. *et al.* Effect of heterogeneous APD restitution on VF organization in a model of the human ventricles. *Am. J. Physiol. Heart Circ. Physiol.* **294,** H764-74 (2008).

39. Yuan, S., Wohlfart, B., Olsson, S. B. & Blomström-Lundqvist, C. The dispersion of repolarization in patients with ventricular tachycardia. A study using simultaneous monophasic action potential recordings from two sites in the right ventricle. *Eur. Heart J.* **16,** 68–76 (1995).

40. Kuo, C. S., Munakata, K., Reddy, C. P. & Surawicz, B. Characteristics and possible mechanism of ventricular arrhythmia dependent on the dispersion of action potential durations. *Circulation* **67,** 1356–67 (1983).

41. Kuo, C. S., Reddy, C. P., Munakata, K. & Surawicz, B. Mechanism of ventricular arrhythmias caused by increased dispersion of repolarization. *Eur. Heart J.* **6 Suppl D,** 63–70 (1985).

42. Habbab, M. A. & el-Sherif, N. Drug-induced torsades de pointes: role of early afterdepolarizations and dispersion of repolarization. *Am. J. Med.* **89,** 241–6 (1990).

43. Pak, H.-N. *et al.* Spatial dispersion of action potential duration restitution kinetics is associated with induction of ventricular tachycardia/fibrillation in humans. *J. Cardiovasc. Electrophysiol.* **15,** 1357–63 (2004).

44. Akar, F. G. Unique Topographical Distribution of M Cells Underlies Reentrant Mechanism of Torsade de Pointes in the Long-QT Syndrome. *Circulation* **105,** 1247–1253 (2002).

45. Sun, L. *et al.* A preliminary study on atrial epicardial mapping signals based on Graph Theory. *Med. Eng. Phys.* **36,** 875–81 (2014).

46. Hohnloser, S. H. & Li, Y. G. Drug treatment of atrial fibrillation: what have we learned? *Curr. Opin. Cardiol.* **12,** 24–32 (1997).

47. Ravens, U., Poulet, C., Wettwer, E. & Knaut, M. Atrial selectivity of antiarrhythmic drugs. *J. Physiol.* **591,** 4087–97 (2013).

48. Boriani, G. *et al.* Atrial antitachycardia pacing and managed ventricular pacing in bradycardia patients with paroxysmal or persistent atrial tachyarrhythmias: the MINERVA randomized multicentre international trial. *Eur. Heart J.* **35,** 2352–62 (2014).

49. Tracy, C. M. *et al.* 2012 ACCF/AHA/HRS focused update of the 2008 guidelines for device-based therapy of cardiac rhythm abnormalities: a report of the American College of Cardiology Foundation/American Heart Association Task Force on Practice Guidelines and the Heart Rhythm S. *Circulation* **126,** 1784–800 (2012).

50. Ginks, M. R. *et al.* Benefits of Endocardial and Multisite Pacing Are Dependent on the Type of Left Ventricular Electric Activation Pattern and Presence of Ischemic Heart Disease: Insights from Electroanatomic Mapping. *Circ. Arrhythmia Electrophysiol.* **5,**

889–897 (2012).

51. Narayan, S. M. *et al.* Treatment of atrial fibrillation by the ablation of localized sources: CONFIRM (Conventional Ablation for Atrial Fibrillation With or Without Focal Impulse and Rotor Modulation) trial. *J. Am. Coll. Cardiol.* **60,** 628–36 (2012).

52. Viventi, J. *et al.* A conformal, bio-interfaced class of silicon electronics for mapping cardiac electrophysiology. *Sci. Transl. Med.* **2,** 24ra22 (2010).

53. Shajahan, T. K., Sinha, S. & Pandit, R. Spiral-wave dynamics depend sensitively on inhomogeneities in mathematical models of ventricular tissue. *Phys. Rev. E. Stat. Nonlin. Soft Matter Phys.* **75,** 011929 (2007).

54. Winfree, A. T. *The Geometry of Biological Time*. (Springer Science & Business Media, 2001).

55. Higgins, J. P. Nonlinear systems in medicine. *Yale J. Biol. Med.* **75,** 247–60 (2002).

56. Honerkamp, J. The heart as a system of coupled nonlinear oscillators. *J. Math. Biol.* **18,** 69–88 (1983).

57. Shajahan, T. K., Sinha, S. & Pandit, R. in *Complex Dynamics in Physiological Systems: From Heart to Brain* (eds. Dana, S. K., Roy, P. K. & Kurths, J.) 51–67 (Springer Netherlands, 2009). doi:10.1007/978-1-4020-9143-8

58. Sinha, S., Pande, A. & Pandit, R. Defibrillation via the elimination of spiral turbulence in a model for ventricular fibrillation. *Phys. Rev. Lett.* **86,** 3678–81 (2001).

59. Sridhar, S. & Sinha, S. Controlling spatiotemporal chaos in excitable media using an array of control points. *EPL (Europhysics Lett.* **81,** 50002 (2008).

60. Rappel, W.-J., Zaman, J. A. B. & Narayan, S. M. Mechanisms for the Termination of Atrial Fibrillation by Localized Ablation: Computational and Clinical Studies. *Circ. Arrhythm. Electrophysiol.* **8,** 1325–33 (2015).

61. Shajahan, T. K., Nayak, A. R. & Pandit, R. Spiral-wave turbulence and its control in the presence of inhomogeneities in four mathematical models of cardiac tissue. *PLoS One* **4,** e4738 (2009).

62. Sinha, S. & Sridhar, S. in *Complex Dynamics in Physiological Systems: From Heart to Brain* (eds. Dana, S. K., Roy, P. K. & Kurths, J.) 69–87 (Springer Netherlands, 2009). doi:10.1007/978-1-4020-9143-8

63. Murphy, S. V & Atala, A. 3D bioprinting of tissues and organs. *Nat. Biotechnol.* **32,** 773–785 (2014).

64. Wan, L. Q. *et al.* Micropatterned mammalian cells exhibit phenotype-specific left-right asymmetry. *Proc. Natl. Acad. Sci. U. S. A.* **108,** 12295–300 (2011).

65. Steinberg, B. E., Glass, L., Shrier, A. & Bub, G. The role of heterogeneities and intercellular coupling in wave propagation in cardiac tissue. *Philos. Trans. R. Soc. A Math. Phys. Eng. Sci.* **364,** 1299–1311 (2006).

66. Chang, M. G. *et al.* Spiral waves and reentry dynamics in an in vitro model of the healed infarct border zone. *Circ. Res.* **105,** 1062–71 (2009).

67. Kanu, U., Iravanian, S., Gilmour, R. F. & Christini, D. J. Control of action potential duration alternans in canine ventricular tissue. *Conf. Proc. ... Annu. Int. Conf. IEEE Eng. Med. Biol. Soc. IEEE Eng. Med. Biol. Soc. Annu. Conf.* **2010,** 1997–2000 (2010).

68. Abilez, O. J. *et al.* Multiscale computational models for optogenetic control of cardiac function. *Biophys. J.* **101,** 1326–34 (2011).

69. Burton, R. A. B. *et al.* Optical control of excitation waves in cardiac tissue. *Nat. Photonics* **9,** 813–816 (2015).

70. Boyden, E. S., Zhang, F., Bamberg, E., Nagel, G. & Deisseroth, K. Millisecond-timescale, genetically targeted optical control of neural activity. *Nat. Neurosci.* **8,** 1263–8 (2005).

71. Govorunova, E. G., Sineshchekov, O. A., Janz, R., Liu, X. & Spudich, J. L. Natural light-gated anion channels: A family of microbial rhodopsins for advanced optogenetics. *Science (80-.).* **349,** (2015).

72. Lin, J. Y., Knutsen, P. M., Muller, A., Kleinfeld, D. & Tsien, R. Y. ReaChR: a red-shifted variant of channelrhodopsin enables deep transcranial optogenetic excitation.

Nat. Neurosci. **16,** 1499–508 (2013).

73. Mezzanotte, L., van 't Root, M., Karatas, H., Goun, E. A. & Löwik, C. W. G. M. In Vivo Molecular Bioluminescence Imaging: New Tools and Applications. *Trends Biotechnol.* **35,** 640–652 (2017).

74. Nihongaki, Y., Kawano, F., Nakajima, T. & Sato, M. Photoactivatable CRISPR-Cas9 for optogenetic genome editing. *Nat. Biotechnol.* **33,** 755–760 (2015).

75. Thomson, J. A. *et al.* Embryonic stem cell lines derived from human blastocysts. *Science* **282,** 1145–1147 (1998).

76. Takahashi, K. & Yamanaka, S. Induction of pluripotent stem cells from mouse embryonic and adult fibroblast cultures by defined factors. *Cell* **126,** 663–676 (2006).

77. Yu, J. *et al.* Induced pluripotent stem cell lines derived from human somatic cells. *Science* **318,** 1917–20 (2007).

78. Takahashi, K. *et al.* Induction of pluripotent stem cells from adult human fibroblasts by defined factors. *Cell* **131,** 861–72 (2007).

79. Dimos, J. T. *et al.* Induced pluripotent stem cells generated from patients with ALS can be differentiated into motor neurons. *Science* **321,** 1218–21 (2008).

80. Ebert, A. D. *et al.* Induced pluripotent stem cells from a spinal muscular atrophy patient. *Nature* **457,** 277–280 (2009).

81. Burridge, P. W. *et al.* Chemically defined generation of human cardiomyocytes. *Nat. Methods* **11,** 855–860 (2014).

82. Yun, S. H. & Kwok, S. J. J. Light in diagnosis, therapy and surgery. *Nat. Biomed. Eng.* **1,** s41551-016-0008-016 (2017).

83. Huang, F. *et al.* Video-rate nanoscopy using sCMOS camera–specific single-molecule localization algorithms. *Nat. Methods* **10,** 653–658 (2013).

84. Dudley, D., Duncan, W. M. & Slaughter, J. Emerging digital micromirror device (DMD) applications. in *Proc. SPIE 4985, MOEMS Display and Imaging Systems, (20*

January 2003) (ed. Urey, H.) **4985,** 14 (International Society for Optics and Photonics, 2003).

85. Nagel, G. *et al.* Channelrhodopsin-2, a directly light-gated cation-selective membrane channel. *Proc. Natl. Acad. Sci. U. S. A.* **100,** 13940–5 (2003).

86. Gradinaru, V., Thompson, K. R. & Deisseroth, K. eNpHR: a Natronomonas halorhodopsin enhanced for optogenetic applications. *Brain Cell Biol.* **36,** 129–39 (2008).

87. Yazawa, M. *et al.* Using induced pluripotent stem cells to investigate cardiac phenotypes in Timothy syndrome. *Nature* **471,** 230–4 (2011).

88. Song, L. *et al.* Dual Optical Recordings for Action Potentials and Calcium Handling in Induced Pluripotent Stem Cell Models of Cardiac Arrhythmias Using Genetically Encoded Fluorescent Indicators. *Stem Cells Transl. Med.* **4,** 468–475 (2015).

89. Vinson, M., Pertsov, A. & Jalife, J. Anchoring of vortex filaments in 3D excitable media. *Phys. D Nonlinear Phenom.* **72,** 119–134 (1994).

90. Lim, Z. Y., Maskara, B., Aguel, F., Emokpae, R. & Tung, L. Spiral wave attachment to millimeter-sized obstacles. *Circulation* **114,** 2113–21 (2006).

91. Bingen, B. O. *et al.* Prolongation of minimal action potential duration in sustained fibrillation decreases complexity by transient destabilization. *Cardiovasc. Res.* **97,** 161–170 (2013).

92. Garrey, W. E. The nature of fibrillatory contraction of the heart: its relation to tissue mass and form. *Am. J. Physiol.* **33,** 397–474 (1914).

93. Zou, R., Kneller, J., Leon, L. J. & Nattel, S. Substrate size as a determinant of fibrillatory activity maintenance in a mathematical model of canine atrium. *AJP Hear. Circ. Physiol.* **289,** H1002–H1012 (2005).

94. Vaidya, D., Morley, G. E., Samie, F. H. & Jalife, J. Reentry and fibrillation in the mouse heart. A challenge to the critical mass hypothesis. *Circ. Res.* **85,** 174–81 (1999).

95. Panfilov, A. V. Is heart size a factor in ventricular fibrillation? Or how close are rabbit

and human hearts? *Hear. Rhythm* **3,** 862–864 (2006).

96. Spach, M. S., Dolber, P. C. & Heidlage, J. F. Influence of the passive anisotropic properties on directional differences in propagation following modification of the sodium conductance in human atrial muscle. A model of reentry based on anisotropic discontinuous propagation. *Circ. Res.* **62,** 811–32 (1988).

97. Spach, M. S. & Josephson, M. E. Initiating reentry: the role of nonuniform anisotropy in small circuits. *J. Cardiovasc. Electrophysiol.* **5,** 182–209 (1994).

98. Kohl, P. & Gourdie, R. G. Fibroblast-myocyte electrotonic coupling: does it occur in native cardiac tissue? *J. Mol. Cell. Cardiol.* **70,** 37–46 (2014).

99. Quinn, T. A. *et al.* Electrotonic coupling of excitable and nonexcitable cells in the heart revealed by optogenetics. *Proc. Natl. Acad. Sci. U. S. A.* **113,** 14852–14857 (2016).

100. Nyns, E. C. A. *et al.* Optogenetic termination of ventricular arrhythmias in the whole heart: towards biological cardiac rhythm management. *Eur. Heart J.* **38,** ehw574 (2016).

101. Watanabe, M. *et al.* Optogenetic manipulation of anatomical re-entry by light-guided generation of a reversible local conduction block. *Cardiovasc. Res.* **113,** 354–366 (2017).

102. Feola, I. *et al.* Localized Optogenetic Targeting of Rotors in Atrial Cardiomyocyte Monolayers. *Circ. Arrhythm. Electrophysiol.* **10,** e005591 (2017).

103. Williams, J. C. & Entcheva, E. Optogenetic versus Electrical Stimulation of Human Cardiomyocytes: Modeling Insights. *Biophys. J.* **108,** 1934–45 (2015).

104. Ronaldson-Bouchard, K. *et al.* Advanced maturation of human cardiac tissue grown from pluripotent stem cells. *Nature* **556,** 239–243 (2018).

105. Si-Tayeb, K. *et al.* Highly efficient generation of human hepatocyte-like cells from induced pluripotent stem cells. *Hepatology* **51,** 297–305 (2010).

106. Zhang, F. *et al.* Multimodal fast optical interrogation of neural circuitry. *Nature* **446,**

633–9 (2007).

107. Burridge, P. W., Holmström, A. & Wu, J. C. Chemically Defined Culture and Cardiomyocyte Differentiation of Human Pluripotent Stem Cells. *Curr. Protoc. Hum. Genet.* **87,** 21.3.1-21.3.15 (2015).

APPENDIX: PUBLISHED WORK

The work shown here represents one part of my overall PhD work, which was broadly located at the intersection of my own personal background in electrical engineering, and the expertise of this laboratory in stem cells and tissue engineering. During my PhD, I had the privilege of working with a number of talented individuals on a wide range of projects including cardiac tissue engineering and maturation, neuromuscular junction formation, immunomodulation, lung regeneration, bioluminescence, image processing, and the work described in this dissertation focusing on cardiac arrhythmias. The following publications and presentations resulted from these efforts.

First author publications:

Ma SP, Vila OF, Kim J, Song LJ, Huang D, Chiang H, Leong K, Yazawa M, Vunjak-Novakovic G. Spatiotemporal control of arrhythmias in human cardiac cell models through optogenetics. ***Circulation Research.*** Submitted.

Ma SP, Shen CY, White EC, Vila OF, Chen TH, Vunjak-Novakovic G. Optogenetic Stimulation for the Maturation of Human Induced Pluripotent Stem Cell-Derived Cardiomyocytes. In preparation.

Ma SP, and Vunjak-Novakovic G. Tissue-Engineering for the Study of Cardiac Biomechanics. ***Journal of Biomechanical Engineering***. January 27, 2016.

Middle author publications:

Guenthart BA, O'Neill JD, Chicotka S, Kim J, Fung K, Queen D, Salna M, Simpson M, Marboe C, Donocoff R, Ma SP, Vila OF, Cunningham K, Chen Ya-Wen, Wobma H, Snoeck HW, Vunjak-Novakovic G, Bacchetta M. Recovery and regeneration of severely damaged lungs using an interventional cross-circulation platform. ***Nature Medicine.*** Submitted.

Vila OF, Uzel SGM, Ma SP, Williams D, Kamm RD, Vunjak-Novakovic G. Maturation and Disease of Human Neuromuscular Connectivity Revealed through Optogenetics. ***Theranostics*** (in review)

Ronaldson-Bouchard K, Ma SP, Yeager K, Chen T, Song LJ, Sirabella D, Morikawa K, Teles D, Yazawa M, Vunjak-Novakovic G. Advanced maturation of human cardiac tissue grown from pluripotent stem cells. ***Nature.*** April 4, 2018.

Wobma HM, Kanai M, Ma SP, Shih Y, Li HW, Duran-Struuck R, Winchester R, Goeta S, Brown LM, Vunjak-Novakovic G. Dual IFN-γ/hypoxia priming enhances immunosuppression of mesenchymal stromal cells through regulatory proteins and metabolic mechanisms. ***Journal of Immunology and Regenerative Medicine***. March 2018.

Vila OF, Garrido C, Cano I, Guerra-Rebollo M, Navarro M, Mecca-Cortés O, Ma SP, Engel E, Rubio N, Blanco J. Real-time bioluminescence imaging of cell distribution, growth and

differentiation in a three-dimensional scaffold under interstitial perfusion for Tissue Engineering. ***Tissue Engineering Part C Methods.*** June 23, 2016.

Published conference abstracts:

Shen CY, Ma SP, White EC, Vila OF, Chen TH, Yeager K, Vunjak-Novakovic G. Optogenetics for the Maturation of hiPS-CMs. ***Tissue Engineering Part A*** 2017 Dec 1 (Vol. 23, pp. S129-S129)

Kim J, Guenthart B, O'Neill JD, Ma SP, Bacchetta M, Vunjak-Novakovic G. An Autonomous Bronchoscope for Drug Delivery into Target Regions in the Lungs. ***Tissue Engineering Part A*** 2017 Dec 1 (Vol. 23, pp. S156-S157)

Ma SP, Vila OF, Vunjak-Novakovic G. Spatiotemporal Control of Human Cardiac Tissue Using an Optogenetic Platform. ***Tissue Engineering Part A*** 2016 Dec 1 (Vol. 22, pp. S26-S26).

Vila OF, Uzel S, Ma SP, Kamm RD, Vunjak-Novakovic G. An Optogenetic 3D Model of Human Neuromuscula Junctions. ***Tissue Engineering Part A*** 2016 Dec 1 (Vol. 22, pp. S24-S24).

Wobma HM, Kanai M, Ma SP, Nakazawa KR, Duran-Struuk R, Li HW and Vunjak-Novakovic G. Preconditioning Mesenchymal Stem Cells to Improve Transplant Tolerance. ***Biology of Blood and Bone Marrow Transplantation*** 22(3): S149-S149, 2016

Wobma HM, Ma SP, Fang J, Vasavada H, Duran-Struuk R, Winchester R, Hirshi K. and Vunjak-Novakovic G. Protection of Organ Vasculature By Endothelial Overexpression of HLA-G. ***Biology of Blood and Bone Marrow Transplantation*** 22(3): S362-S362, 2016.

First author oral presentations:

Ma SP, Vila OF, Kim J, Chiang H, Yazawa M, Vunjak-Novakovic G. Spatiotemporal Control of Human Cardiac Tissue Using an Optogenetic Platform. ***Biomedical Engineering Society (BMES) Annual Meeting***, Phoenix, Arizona, October 11-14, 2017.

Ma SP, Vila OF, Vunjak-Novakovic, G. Spatiotemporal Control of Human Cardiac Tissue Using an Optogenetic Platform. ***Tissue Engineering and Regenerative Medicine International Society-Americas (TERMIS-AM) Annual Conference and Exhibition***, San Diego, CA, December 11-14, 2016.

First author poster presentations:

Ma SP, Vila OF, Kim J, Chiang H, White EC, Shen CY, Yazawa, M, Vunjak-Novakovic G. Spatiotemporal Control of Human Cardiac Tissue Using an Optogenetic Platform. ***New York Stem Cell Science Program (NYSTEM) Annual Meeting***, New York, NY, May 11-12, 2017.

Ma SP, Vila OF, Vunjak-Novakovic G. Optogenetics for tissue engineering applications. ***Poster Presentation, New York Stem Cell Science Program (NYSTEM) Annual Meeting***, New York, NY, May 10-11, 2016.